NAVAL POSTGRADUATE SCHOOL
Monterey, California

THESIS

EFFECT OF THERMAL RESIDUAL STRESSES
ON THE STRESS-STRAIN BEHAVIOR OF
METAL-MATRIX COMPOSITES

by

John D. Sims

September 1990

Thesis Advisor I. Dutta

Approved for public release; distribution is unlimited.

REPORT DOCUMENTATION PAGE

Report Security Classification Unclassified		1b Restrictive Markings	
Security Classification Authority		3 Distribution Availability of Report Approved for public release; distribution is unlimited.	
Declassification Downgrading Schedule			
Performing Organization Report Number(s)		5 Monitoring Organization Report Number(s)	
Name of Performing Organization aval Postgraduate School	6b Office Symbol *(if applicable)* 33	7a Name of Monitoring Organization Naval Postgraduate School	
Address *(city, state, and ZIP code)* lonterey, CA 93943-5000		7b Address *(city, state, and ZIP code)* Monterey, CA 93943-5000	
Name of Funding Sponsoring Organization	8b Office Symbol *(if applicable)*	9 Procurement Instrument Identification Number	
Address *(city, state, and ZIP code)*		10 Source of Funding Numbers	
		Program Element No	Project No / Task No / Work Unit Accession No

Title *(include security classification)* EFFECT OF THERMAL RESIDUAL STRESSES ON THE STRESS-STRAIN BEAVIOR OF METAL-MATRIX COMPOSITES

Personal Author(s) John D. Sims

a Type of Report	13b Time Covered	14 Date of Report *(year, month, day)*	15 Page Count
laster's Thesis	From To	September 1990	69

Supplementary Notation The views expressed in this thesis are those of the author and do not reflect the official policy or poion of the Department of Defense or the U.S. Government.

Cosati Codes			18 Subject Terms *(continue on reverse if necessary and identify by block number)*
eld	Group	Subgroup	thermal stresses, composites, finite element

Abstract *(continue on reverse if necessary and identify by block number)*

A parametric study was conducted to assess the effect of thermal residual stresses on the stress-strain response of a fiber-inforced metal-matrix composite. The material chosen for investigation was the SiC-whisker reinforced Al 6061 system. ne effects of fiber volume fraction, fiber aspect ratio and fiber spacing were analyzed within the framework of axisymmetric nite-element models to determine the overall constitutive response of the composite as well as to solve for local field quanies in the fiber and matrix. The composite was modeled as a periodic array of cylindrical fibers, laterally aligned in one odel and staggered in the other. Perfect interfacial bonding and complete fiber alignment with the tensile axis were assumed. ne results indicated that (1) composite stiffness, yield strength and work-hardening rate increased with increasing volume nction and fiber aspect ratio and (2) variations in fiber spacing primarily affect work-hardening rate and have negligible effect n composite stiffness. It was found that the presence of residual stresses affected the stress-strain behavior of the composite r influencing the load transfer characteristics between the matrix and fiber as well as the initiation and growth of plastic formation in the matrix.

Distribution Availability of Abstract unclassified unlimited ☐ same as report ☐ DTIC users	21 Abstract Security Classification Unclassified	
a Name of Responsible Individual Dutta	22b Telephone *(include Area code)* (408) 646-2851	22c Office Symbol ME/Du

) FORM 1473,84 MAR 83 APR edition may be used until exhausted
All other editions are obsolete

security classification of this page

Unclassified

Approved for public release; distribution is unlimited.

Effect of Thermal Residual Stresses on the Stress-Strain Behavior of Metal-Matrix Composites

by

John D. Sims
Lieutenant , United States Navy
B.S., University of Florida, 1984

Submitted in partial fulfillment of the
requirements for the degree of

MASTER OF SCIENCE IN MECHANICAL ENGINEERING

from the

NAVAL POSTGRADUATE SCHOOL
September 1990

ABSTRACT

A parametric study was conducted to assess the effect of thermal residual stresses on the stress-strain response of a fiber-reinforced metal-matrix composite. The material chosen for investigation was the SiC-whisker reinforced Al 6061 system. The effects of fiber volume fraction, fiber aspect ratio and fiber spacing were analyzed within the framework of axisymmetric finite-element models to determine the overall constitutive response of the composite as well as to solve for local field quantities in the fiber and matrix. The composite was modeled as a periodic array of cylindrical fibers, laterally aligned in one model and staggered in the other. Perfect interfacial bonding and complete fiber alignment with the tensile axis were assumed. The results indicated that (1) composite stiffness, yield strength and work-hardening rate increased with increasing volume fraction and fiber aspect ratio and (2) variations in fiber spacing primarily affect work-hardening rate and have negligible effect on composite stiffness. It was found that the presence of residual stresses affected the stress-strain behavior of the composite by influencing the load transfer characteristics between the matrix and fiber as well as the initiation and growth of plastic deformation in the matrix.

TABLE OF CONTENTS

I. INTRODUCTION 1
A. THERMAL RESIDUAL STRESSES IN METAL-MATRIX COMPOSITES 1
B. STRESS-STRAIN BEHAVIOR OF METAL-MATRIX COMPOSITES ... 5
C. RESEARCH OBJECTIVES AND OVERVIEW 8

II. EXPERIMENTAL APPROACH 10
A. NUMERICAL MODELING 10
1. Finite Element Modeling 12
2. Boundary Conditions 15
3. Applied Loading 17
4. Grid Independence 18
5. Model Implementation 19
B. MATERIAL TESTING 19

III. RESULTS AND DISCUSSION 21
A. COMPARISON OF ALIGNED AND STAGGERED FIBER MODELS . 21
B. EFFECT OF FIBER VOLUME FRACTION 25
C. EFFECT OF FIBER ASPECT RATIO 25
D. EFFECT OF FIBER SPACING 31
E. EFFECT OF THERMAL RESIDUAL STRESSES 31
F. PLASTIC ZONE INITIATION AND GROWTH 36
1. Thermal Residual Stress Effects 36
2. Volume Fraction Effects 38
3. Effects of Modeling Constraints 41
4. Fiber Spacing Effects 43

IV. CONCLUSIONS 46

APPENDIX A. SAMPLE ADINA INPUT FILE 47

APPENDIX B. ADINA MODIFICATIONS FOR STAGGERED FIBER MODEL 51

APPENDIX C. DATA REDUCTION PROGRAMS 53

LIST OF REFERENCES 57

INITIAL DISTRIBUTION LIST 60

LIST OF FIGURES

Figure 1. Optical Micrograph 11
Figure 2. Material Representations 14
Figure 3. Modeling Constraint Effects 22
Figure 4. Volume Fraction Effects 26
Figure 5. Fiber Aspect Ratio Effects 27
Figure 6. Effect of the Critical Fiber Aspect Ratio 28
Figure 7. Fiber Load-Bearing Behavior 29
Figure 8. Fiber Spacing Effects 32
Figure 9. Residual Stress and Volume Fraction Effects 33
Figure 10. Residual Stress and Modeling Constraint Effects 35
Figure 11. Plastic Zone Development-Residual Stress Effects 37
Figure 12. Plastic Zone Development-Volume Fraction Effects 39
Figure 13. Plastic Zone Development-Constraint Effects 42
Figure 14. Plastic Zone Development-Fiber Spacing Effects 44

ACKNOWLEDGEMENTS

This author would like to take the opportunity to express his gratitude to several individuals who have been influential in the successful completion of this thesis. First, I would like to thank Professor Dutta for his patience and guidance throughout the course of the study. Professor Salinas was instrumental, not only as a first-rate instructor, but also as an honest critic of this manuscript. Professor Cantin was influential in the selection of ADINA as the software of choice to conduct the finite-element analysis. David Marco, Tom McCord and Charles Crow were of great assistance in providing computer support and fabricating material samples.

Of all those deserving credit for their role in this study, the one person most responsible for its completion and quality is my wife, Kristen. She patiently endured the long hours of time spent away from home and was always ready with a word of encouragement when results had gone awry.

I. INTRODUCTION

Metal matrix composites are materials that combine a relatively soft metallic matrix with a high-strength, high-stiffness reinforcement material that is typically a ceramic, intermetallic, metalloid or metal. These materials are characterized either by the nature or the morphology of the reinforcement. Continuous fiber composites consist of fibers, often in a laminar construction, spanning the entire length of the matrix material. Discontinuous fiber composites consist of short fibers or whiskers arranged in a random fashion in the matrix. The degree of randomness as well as the length of the fibers can be controlled, to an extent, through processing. Other metal matrix composite systems such as particulate, flake and foam composites derive their names from the morphology of the reinforcing material.

Wrought aluminum alloys, such as 2024, 6061 and 7075, reinforced with boron, graphite, alumina or silicon carbide have been used extensively in applications as engine or structural components. Some of the improvements in mechanical properties over the unreinforced matrix include increased elastic modulus, tensile strength, wear resistance, fatigue resistance, strength-to-weight ratio and thermal conductivity.

In order for optimal utilization of metal matrix composites in industry, detailed knowledge of the factors affecting their thermal, electrical and mechanical properties must be known.

A. THERMAL RESIDUAL STRESSES IN METAL-MATRIX COMPOSITES

Thermal residual stresses are generated in metal matrix composites during fabrication due to the coefficient of thermal expansion (CTE) mismatch between the matrix and reinforcing material. The exact nature of these stresses and their effect on the mechanical properties of the composite has been the subject of numerous investigations.

Examples of continuum mechanics applied to a thick-walled cylinder model under internal pressure or containing a continuous fiber abound in the literature. DeSilva and Chadwick [Ref. 1] used a continuous fiber model to investigate dimensional changes due to temperature effects in iron-boron and copper-tungsten composites. Their results indicated that matrix yielding occurred first at the fiber interface then spread radially outward. Dvorak *et al.* [Ref. 2] used a linear elastic continuous fiber model to determine the initial yield surface in the matrix due to temperature changes in the boron-aluminum system. They determined that yielding occurred first at the interface and that a temperature change as small as 10 - 20 °C was sufficient to result in localized yielding in the matrix. Hoffman [Ref. 3] used a continuous fiber model to determine thermal stresses induced during cooldown in the tungsten fiber reinforced 80Ni-20Cr matrix. It was conjectured that the magnitude of these stresses would be sufficient to result in plastic flow in one or both of the constituents. Garmong [Ref. 4] assumed one-dimensional deformation while neglecting shear and poisson effects to calculate matrix stress, strain and plastic work as a function of temperature change. He reported the residual stresses in the matrix as tensile in nature with plastic strains reaching 0.32%. Eammme *et al.* [Refs. 5,6] used a continuum mechanics based approach to investigate the stress states around spherical, misfitting particles of high symmetry under the assumptions of a von Mises yield criterion, linear and power-law strain hardening, and incremental plasticity. Arsenault and Fisher [Ref. 7] used the results of electron microscopy and electron diffraction experiments to conclude that thermal residual stresses in the matrix were caused by CTE mismatch and that matrix strengthening was due to an enhanced dislocation density in the matrix immediately adjacent to the fiber. It was postulated that thermal residual stresses had little effect on matrix strength. In a companion study, Arsenault [Ref. 8] compared experimental results with continuum mechanics predictions and determined that the presence of a discontinuous fiber reinforcement resulted in levels

of strengthening much greater than predicted by theory. The cause of this discrepancy was an enhanced dislocation density due to the CTE mismatch between the materials. Arsenault and Taya [Refs. 9,10] used X-ray diffraction results and yield strength data in tension and compression to determine the extent of thermal residual stresses in a SiC whisker reinforced 6061 Aluminum composite. The experimental results were compared with analytical results obtained using the modified shear-lag theory and the Eshelby equivalent inclusion method. The results indicated that a tensile residual stress existed in the matrix on a volume average basis, although tensile and compressive components were distributed throughout. Both theoretical methods underpredicted the magnitude of strengthening; however the Eshelby method predicted the correct qualitative trends for low fiber aspect ratios. The shear-lag theory was seen as a crude approximation even with the modification by Nardone and Prewo [Ref. 11] to account for tensile load transfer at the fiber tip. A prismatic punching model was developed by Arsenault and Shi [Ref. 12] to attempt to predict the increase in dislocation density in the matrix on cooldown due to CTE mismatch between the constituents. In an exhaustive study, Withers *et al.* [Ref. 13] used the Eshelby method to provide a rigorous theoretical basis for the prediction of mechanical properties in discontinuous fiber composites. The Eshelby model was modified to account somewhat for inclusion shape, geometry and distribution and a full range of elastic, thermo-elastic and plastic composite properties were investigated. The objective of the work was to provide a simple, reliable method, based on the Eshelby theory, to analyze internal stresses in two-phase materials such as metal matrix composites. The mean fiber and matrix stresses were determined as linear functions of applied load and fiber/matrix misfit. The model was used to characterize composite properties such as elastic modulus, CTE, matrix-to-fiber load transfer, thermal residual stress levels and interfacial bond strength. Derby and Walker [Ref. 14]

attempted to characterize the contribution of thermal strains to matrix strength using a combination of electron microscopy and hardness tests.

The use of numerical solution techniques to determine the effect of residual stresses on a microstress level have gained wide appeal among researchers. Dutta *et al.* [Ref. 15] used a combination of continuum methods with finite element analysis to model the deformation zone arising from differential thermal contraction. Models were constructed for periodic arrays of spherical and cylindrical reinforcements. In a follow-on study, Dutta [Ref. 16] used an axisymmetric finite element model to investigate the effect of residual stresses in SiC/Al 6061 composites. The model assumed rigid and elastic fibers with elastic-ideally-plastic matrices. The results indicated that residual stresses are responsible for the less than expected matrix-to-fiber load transfer observed in discontinuously reinforced metal-matrix composites. Povirk *et al.* [Ref. 17] conducted a parametric study of the effects of fiber spacing, volume fraction and fiber aspect ratio on the residual stresses in metal-matrix composites. The composite was modeled as a periodic array of perfectly aligned cylindrical cells, each composed of a cylindrical fiber surrounded by a matrix shell. The analysis accounted for thermo-elastic response in the fiber and thermo-elastic-plastic response in the matrix. A Lagrangian-Jaumann stress rate formulation was used to model the constitutive response of the material. A quenching process was simulated by imposing a temperature history on the cell surface through solution of the heat equation for a cylindrical bar. The results indicated that transverse fiber spacing was the most important microstructural parameter affecting the distribution of residual stress and magnitude of plastic deformation in the matrix. Fiber aspect ratio was seen to have negligible effect on residual stresses since these stresses became independent of axial position a short distance from the fiber corner. The overall level of plastic deformation in the matrix was primarily dependent on the fiber volume fraction.

B. STRESS-STRAIN BEHAVIOR OF METAL-MATRIX COMPOSITES

Several in-depth studies have recently been conducted to investigate the dependence of composite stress-strain behavior on material properties and the size, shape and distribution of the reinforcing phase. These studies have relied almost exclusively on finite element methods to determine the magnitudes of local field quantities and overall deformation behavior. The flexibility afforded by this method enables a wide range of effects to be included in the numerical models that cannot otherwise be accounted for effectively using traditional continuum mechanics theories. Factors such as non-proportional loading and stress concentration zones due to the presence of sharp corners in the reinforcement often render these methods intractable.

Christman *et al.* [Ref. 18] conducted an experimental and numerical study of deformation in metal-ceramic composites with the objective of investigating the dependence of tensile properties on reinforcement shape, aspect ratio and distribution. The numerical analysis was conducted using a Lagrangian kinematic formulation with Jaumann stress rate and strain rate tensors used in the constitutive response. The matrix material was modeled as an elastic viscoplastic solid subject to isotropic work hardening. For the fibers, elastic and perfectly rigid models were used in the analysis. The material model for the composite consisted of a regular, periodic array of perfectly aligned fibers within cylindrical unit cells. The numerical study was carried out within the context of an axisymmetric analysis to account for fiber aspect ratio, fiber spacing, and volume fraction effects; a two dimensional plane strain analysis was used to account for variations in fiber distribution. Two different sets of boundary conditions were applied to the model to simulate geometric constraint effects. The numerical results indicated that significant hydrostatic stress states (up to 6 times the composite offset yield strength) were developed in the matrix during deformation. Plastic deformation occurred first at the fiber tip then spread rapidly throughout the matrix, with the magnitude of the ef-

fective plastic strain greatly exceeding the far-field axial strain. The results of the parametric study were in qualitative agreement with experimental results. Fiber volume fraction was the single greatest factor affecting composite strength. The effects of fiber aspect ratio and spacing were strongly influenced by the geometric constraint imposed on the model and the subsequent hydrostatic stress states developed. To compare the numerical models with experimental tensile data, average values for fiber and cell aspect ratio were chosen from optical microscopy results. The model with imposed sidewall constraint predicted values of elastic modulus, yield strength and tensile strength far in excess of the experimental data. The model without imposed sidewall constraint over-predicted the values of elastic modulus and yield strength, but greatly underpredicted the tensile strength and work-hardening rate of the actual composite.

In two companion studies, Tvergaard [Refs. 19, 20] applied the finite element scheme used by Christman *et al.* [Ref. 18] to investigate the parametric effects of volume fraction, fiber spacing and fiber aspect ratio using a unit cell model in which the fibers were shifted relative to one another. The purpose of this modeling constraint was to account for matrix shearing between adjacent fiber ends. The author postulated that this shearing was a main deformation mechanism in the actual composite. Additionally, fiber debonding was accounted for using a cohesive zone model that described normal and tangential separation as well as fiber pull-out. The qualitative results for the volume fraction, fiber aspect ratio and fiber spacing effects were identical to the previous study, however the effect of matrix shearing due to the shifted fiber arrangement lowered the magnitudes of the strength predictions into much closer agreement with experimental results. The results also indicated that the assumption of rigid fibers was a good approximation for modeling discontinuous fiber composites. The results for the fiber debonding model revealed that interfacial separation occurred first at the fiber corner followed by separation along the top and sidewall fiber surfaces, respectively. The au-

thor predicted that thermal residual stresses would tend to delay the onset of debonding as well as increase Coulombic friction effects once fiber pull-out occurred.

Using three-dimensional finite element models, Levy and Papazian [Ref. 21] investigated the tensile properties of aluminum matrix composites containing whisker and particulate silicon carbide. The SiC fibers were modeled as longitudinally aligned cylinders in a three-dimensional array. The fibers were assumed transversely aligned in one model and staggered in the other. The matrix material was modeled as elastic-plastic and the SiC as elastic. The variables selected for study were fiber volume fraction, fiber aspect ratio, fiber spacing and orientation of the fiber to the applied load. The analytical results accurately predicted the increase in strain hardening rate and elastic modulus with increasing volume fraction and fiber aspect ratio. The models also predicted the experimentally observed initial decrease and subsequent increase in proportional limit with increasing volume fraction. The results of orienting the fiber orthogonal to the applied load indicated little dependence on fiber aspect ratio. The microstress data were used to predict the location and growth of the plastic zone during deformation. The use of three-dimensional analysis allowed the authors to account for the presence of adjacent fibers more accurately than in the typical axisymmetric model. The initial yielding location in longitudinal loading was sensitive to fiber aspect ratio and fiber spacing. For fiber aspect ratios of one, initial yielding in the matrix occurred at the midpoint between adjacent fiber end surfaces. For aspect ratios of four and larger, initial yielding occurred along the fiber end surface. In transverse loading, initial yielding always occurred between adjacent fibers next to the lateral (cylindrical) fiber surfaces.

Brockenbrough and Suresh [Ref. 22] used three-dimensional cylindrical and plane strain models to investigate the sensitivity of plastic deformation behavior of continuous fiber composites to variations in fiber cross-section and distribution. The composite was modeled as a periodic array of three-dimensional unit cells with the fibers arranged in

"square" edge-packing and "hexagonal" edge-packing configurations. Fiber distribution effects were studied using a plane strain model of 26 cylinders of aspect ratio 1. The analytical results indicated that the plastic deformation characteristics of the composite in transverse loading were influenced both by the fiber cross-sectional geometry and distribution. However, fiber distribution had a more pronounced effect on transverse tensile properties. In longitudinal loading, the evolution of matrix triaxiality and plasticity overshadowed both fiber geometry and distribution effects.

C. RESEARCH OBJECTIVES AND OVERVIEW

While the previously discussed research efforts have shed light on the extent and effect of thermal residual stresses on some strengthening mechanisms in metal matrix composites, as well as the sensitivity of composite tensile properties on processing variables, a comprehensive study into the effect of these stresses on the overall stress-strain response is not available in the current literature. Accordingly, the purpose of this research is twofold. The first objective is to investigate the effect of the thermal residual stresses generated in the matrix during cooldown from the fabrication/solutionizing temperature on the uniaxial stress-strain response of the composite. Since these residual stresses are expected to be strongly dependent upon fiber volume fraction, fiber aspect ratio and fiber spacing, the second objective is to conduct a parametric study of the effect of the above factors on composite tensile behavior. The parametric effects of fiber volume fraction, fiber aspect ratio and fiber spacing will be considered within the context of two-dimensional, axisymmetric finite element analysis and compared for the cases of materials with and without residual stresses, respectively. The model system chosen for study is a discontinuous SiC fiber reinforced Al 6061-T6 matrix composite.

Chapter II of this thesis details the assumptions and methods used in the numerical modeling of the composite as well as the material testing procedures. Chapter III con-

tains the results of the investigation and compares the findings with current literature. Chapter IV summarizes the relevant conclusions of the study.

II. EXPERIMENTAL APPROACH

A. NUMERICAL MODELING

In order to accurately describe the behavior of a composite material numerically, the model must contain an appropriate level of realism in the choice of geometric and material variables. Figure 1 is an optical micrograph of a 30 vol.% SiC_w/Al 6061 composite. The photograph reveals several characteristics of the actual composite that need to be considered in attempting to model the material numerically. First, there is a considerable degree of randomness in fiber alignment, with some fibers actually oriented orthogonal to the tensile axis. Takao *et al.* [Ref. 23] investigated the effects of fiber misorientation on the effective elastic modulus of short fiber composites. Using a continuum approach based on the Eshelby method, the authors found that fiber alignment had a greater impact on composite elastic modulus than fiber volume fraction. A second modeling consideration is the non-uniformity in fiber distribution throughout the material. This leads to regions in the matrix in which the fibers are clustered together resulting in a local volume fraction in excess of the bulk volume fraction of the material. Similarly, there are low-fiber concentration regions in which the local mechanical properties of the composite are approximately those of the unreinforced matrix. Previous investigations [Refs. 18,22] have described the effect of fiber clustering within the context of plane strain finite element models. Their results indicated that clustering greatly reduced the resistance to plastic flow in the composite by decreasing the magnitude of matrix triaxiality; however, the elastic properties of the composite were not significantly affected by variations in fiber distribution. A third modeling consideration is the wide range of fiber aspect ratios encountered in the material. A majority of previous studies have attempted to account for this effect by using an average fiber aspect ratio in the

Figure 1. Optical Micrograph: Optical micrograph at 1000x of a 30 vol.% SiC fiber-reinforced Al 6061 composite processed with a 6.5:1 reduction ratio.

numerical calculations. An investigation by Takao and Taya [Ref. 24] revealed that volume averaging resulted in larger values of aspect ratio than a simple frequency-averaging approach. Experimental data was compared with analytical results based on the Eshelby method. For short fiber composites, it was determined that the use of a volume-averaged fiber aspect ratio gave predictions of elastic modulus within 7% and CTE within 10% of experimental values. Additionally, the authors indicated that the wider the range of aspect ratio distribution in the material, the greater the error in the use of an average aspect ratio in analytical results.

1. Finite Element Modeling

In using the finite-element method to predict macro-mechanical composite behavior, an assumption implicit in the modeling is that the behavior of a microscopic portion of the material can adequately represent the behavior of the bulk material. To this end, a multipurpose finite-element code, ADINA, was used to predict macrscopic mechanical behavior in the form of uniaxial stress-strain curves, and microscopic behavior in the form of von Mises effective stress contours plots. ADINA permitted great flexibility in modeling through the use of geometric and materially non-linear solution capabilities. Two-dimensional axisymmetric analysis was used in conjunction with an Updated-Lagrangian-Jaumann (ULJ) kinematic formulation. This numerical scheme uses the principle of virtual work to calculate incremental displacements, which through appropriate constitutive relations yield elemental stresses. The non-linear response of the material is approximated through an incremental approach that predicts the configuration of the body at $t + \Delta t$ with the present configuration at t. In this case, t denotes an iterative counter and not time. This scheme, based on the Newton-Raphson equations [Ref. 25], applies incremental displacements to the body until the applied external load is balanced by the sum of the internal nodal forces. The numerical models were constructed using two-dimensional isoparametric elements. Second-order Gaussian

integration was used to provide suitable numerical accuracy in the solution. The aluminum matrix was characterized by a bilinear stress-strain curve, the slopes of which represent the elastic modulus, E, and strain-hardening modulus, E_t, respectively. The aluminum matrix was assumed to undergo isotropic work hardening and obey the von Mises yield criterion. All material properties were assumed to be constant within the temperature range considered in the study. This is a highly idealized assumption in the case of aluminum; however, for the purposes of this study, room temperature properties were used in view of the modeling of the quench process as an instantaneous event. For aluminum 6061 in the T6 condition, the relevant thermo-mechanical properties are E = 68.3 GPa, E_t = 656 MPa, σ_y = 276 MPa, ν = 0.33 and CTE = 23.0 μK^{-1}; the SiC fiber values are E = 450 GPa, ν = 0.2 and CTE = 4.3 μK^{-1}.

In the present work, two unit cell configurations similar in nature to models of previous researchers [Refs. 18, 19] are considered to account for the cases of aligned fiber (Figure 2a) and staggered fiber (Figure 2b) arrangements, respectively. In each case, the material is assumed to be composed of a periodic array of cylindrical unit cells perfectly aligned with the tensile axis. As shown in Figure 2c, each cell is composed of a cylindrical fiber of radius R_f and length L_f surrounded by a matrix shell of radius R_c and length L_c. In order to simplify computational effort, the three-dimensional problem was reduced to two-dimensions by using an axisymmetric modeling approach. The axisymmetric approximation assumes that a structure with rotational symmetry about an axis in the presence of a rotationally symmetric load can be fully described using a two-dimensional model with a unit radian width [Ref. 26]. From Figure 2c, it can be seen that the axisymmetric model is an appropriate analog to a three-dimensional array of hexagonal unit cells [Ref. 19].

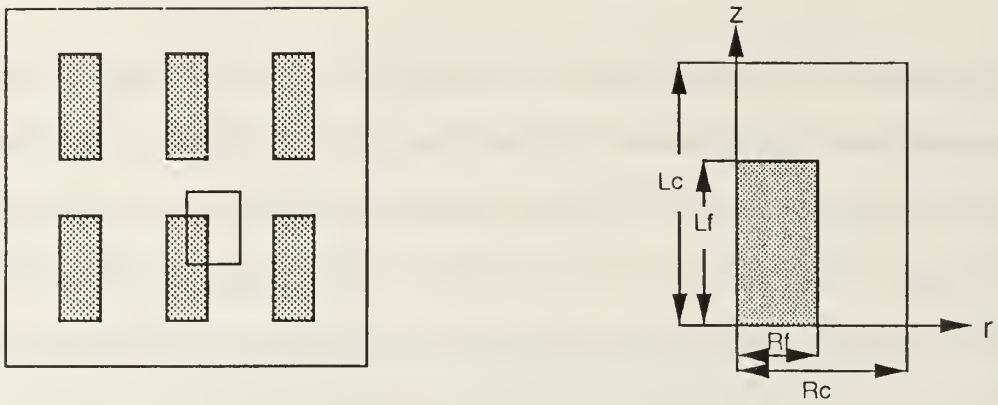

(a)

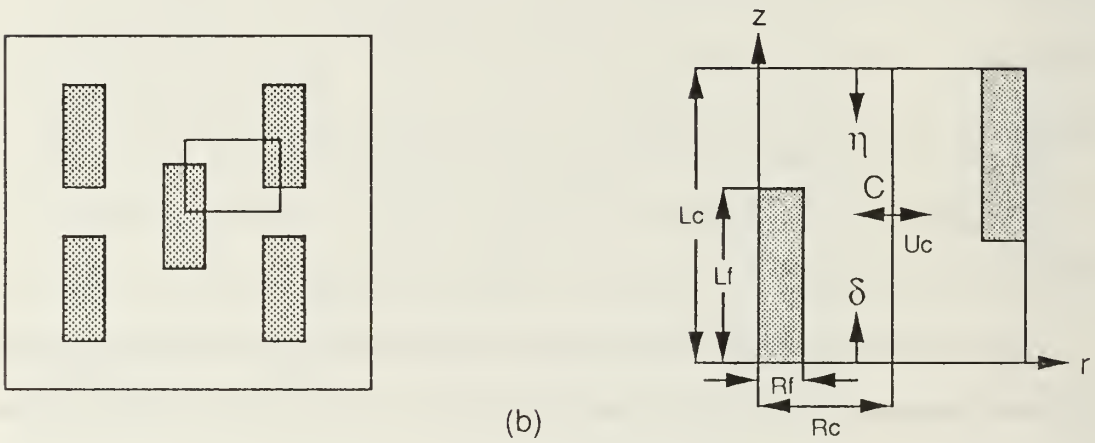

(b)

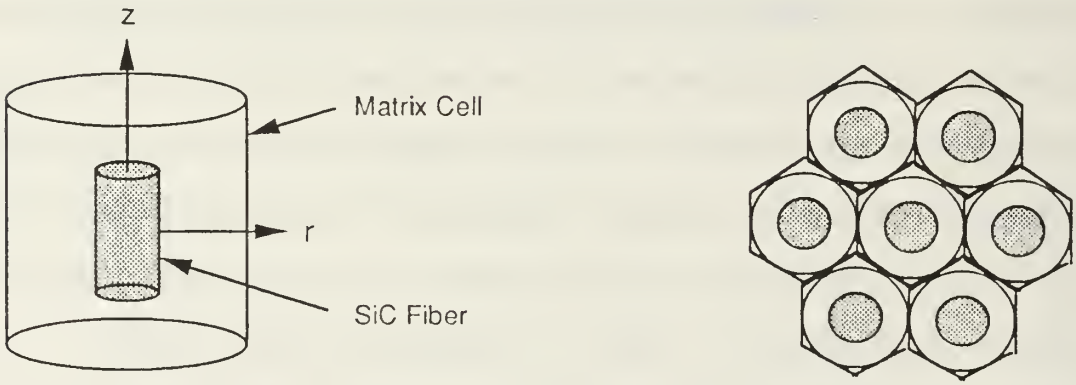

(c)

Figure 2. Material Representations: Diagram showing the (a) aligned fiber and (b) staggered fiber arrangement with associated unit cell configurations and (c) the depiction of the fiber embedded in a matrix shell.

2. Boundary Conditions

In ADINA, displacement-based boundary conditions are specified in addition to a master set of translational and rotational degrees of freedom for the entire finite-element model. In axisymmetric analysis, ADINA requires the model to be contained in the positive quadrant of the y-z plane. The master degrees of freedom in this case allow y and z translation only. Subsequent specifications on displacement boundary conditions can modify, but not delete the master degrees of freedom.

A cylindrical coordinate system was used with displacements u_z and u_r corresponding to the z and r axes, respectively. For the aligned fiber model, two sets of boundary conditions were employed to simulate the effect of neighboring unit cells through the use of geometric constraints. One model was used to simulate a material allowed to undergo unconstrained plastic flow. The only boundary conditions required for this case are $u_z = 0$ along $z = 0$ and $u_r = 0$ along $r = 0$. These conditions describe a cell in which deformation response is unaffected by the presence of neighboring cells. While such a condition is physically impossible, its value as a numerical model is in serving as a comparison to assess the role of varying degrees of geometric constraint on composite constitutive response.

For the aligned fiber model "constrained" by adjacent unit cells, the boundary conditions, in addition to those for the "unconstrained" case, require that the displacements u_z on $z = L_c$ and u_r on $r = R_c$ be constrained to preserve the right circular cylindrical shape of the unit cell throughout the deformation history of the material. In this case, the cell "senses" the presence of neighboring cells by application of additional constraints at the top and lateral surfaces of the cell such that they remain planar throughout the quench and tensile loading process.

The staggered fiber model (Figure 2b) depicts the composite as a periodic array of fibers perfectly aligned with the tensile axis, yet shifted relative to one another along

the z-direction. This model is complicated by the necessity of including the combined effects of two adjacent unit cells in the boundary conditions. Due to the unique arrangement of the cells, the top surface of one cell is constrained to move not only in a plane, but also only as much as the bottom surface of the adjacent cell. Since this bottom surface contains the fiber, this portion of the cell will contract far less during the quench. The requirement for top and bottom surface displacements to be equal and opposite imposes greater constraint on the cell than in the aligned "with constraint" case. Along the cell centerline, symmetry conditions require that $u_r = 0$ along r = 0. On the lateral surface of the cell at r = R_c, compatibility requirements in the axial direction require that the u_z displacements above and below point C be equal and opposite since this point is the geometric center of the two cell system. In the radial direction, the situation is complicated by the necessity to constrain the movement of the nodes above and below point C as a function of the radial displacement of point C (u_c) to ensure that the total cross-sectional area of the two cell system remain independent of the axial coordinate. Tvergaard [Ref. 19] applied this boundary condition by requiring

$$\{u_r(\eta) + R_c\}^2 + \{u_r(\delta) + R_c\}^2 = 2\{u_c + R_c\}^2 \qquad (1)$$

where the coordinates η and δ correspond to the local coordinate systems of the top and bottom cell surfaces, respectively. The displacement-based boundary modeling capabilities of ADINA preclude meeting this requirement explicitly, hence radial compatibility is relaxed somewhat in the staggered model.

The staggered model boundary conditions are an important counterpart to the aligned models in that the effects of matrix shearing due to overlapping fibers on the plastic deformation behavior of the composite can be studied. Due to the non-uniformity of fiber distribution in the material, actual composite response will be a combination of both aligned and staggered fiber configurations.

Perfect bonding is assumed along the fiber-matrix interface. This is accomplished in ADINA by specifying that the fiber and matrix elements adjacent to the interface share the boundary nodes, thereby precluding the possibility of separation during the loading sequence.

3. Applied Loading

The loading scheme used in the numerical modeling combines thermal and displacement loads in a sequence designed to approximate those experienced by the composite during fabrication and subsequent tensile testing.

The cooldown from the fabrication/solutionizing temperature to room temperature is accomplished by subjecting all nodes in the unit cell to a 505 °C temperature drop in one solution time step. In ADINA this is accomplished by selecting the incremental time step size to be equal to the solution time period, thereby bringing the nodal temperatures from the solutionizing temperature (530 °C) to room temperature (25 °C) in one step. The rationale for adopting this approach was to: (1) eliminate the effect of quench rate from the solution and (2) eliminate size and bulk thermal property effects necessary when attempting to impose a thermal history at the surfaces of the unit cell. While this analysis does not take into account factors such as thermal softening due to heat generation during plastic deformation, it was assumed that the dominant effect on the composite from the fabrication cycle is the generation of an enhanced dislocation density in the vicinity of the fiber-matrix interface that is primarily a factor of CTE mismatch. The resulting nodal displacements from the quench were stored in a restart file to be used as initial nodal displacements during tensile loading analysis. The use of restart analysis allows great flexibility in modeling by permitting the use of a variety of loading conditions in a sequence, thereby providing a more realistic simulation of real processes.

Tensile loading of the model was accomplished by applying an axial displacement of

$$\Delta L_c = (e^{\varepsilon} - 1)L_c \tag{2}$$

where ε is the applied true strain. For the aligned model, ΔL_c was applied to the top surface of the unit cell; in the staggered case, a displacement of $\frac{\Delta L_c}{2}$ was applied to the top and bottom surfaces, respectively. The composite stress-strain curves were constructed by applying a ΔL_c corresponding to a selected value of ε. The average axial stress was calculated using a volume-average approach as follows:

$$\sigma_{zz}^{c} = \frac{1}{V_c}\int \sigma_{zz}^{f} dV_f + \frac{1}{V_c}\int \sigma_{zz}^{m} dV_m \tag{3}$$

where superscripts c, f and m correspond to composite, fiber and matrix values, respectively. In this equation, each σ_{zz} represents an average of the four stress values obtained from the Gaussian integration points within each finite-element. The average elemental stresses are then multiplied by their corresponding elemental volumes and summed over the entire volume of the composite.

4. Grid Independence

In order to obtain accurate solutions from a numerical model, convergence criteria for the linearization process and the mesh geometry must be established. In ADINA, the user has the option of selecting the iterative scheme for linearization, the basis for convergence (displacement, energy, etc.) and the value for the convergence criterion. For the Full-Newton iterative scheme selected for use in this study, out-of-balance energy was the basis for convergence and the required tolerance was set to 10^{-6}. The mesh for each model was uniformly refined until 2 successive values of σ_{zz}^{c} at

$\varepsilon = 0$ (the residual axial stress) gave results that agreed to within 10%. The residual axial stress value was found to be the factor most sensitive to changes in mesh size and, therefore, was determined to be the most suitable parameter to establish grid independence. In most cases, the numerical models achieved grid independence with approximately 250 elements.

5. Model Implementation

The numerical models discussed above were modified for the particular variable whose effect was being evaluated. The models used to approximate the 30 vol.% experimental data were assigned values of fiber and cell aspect ratios of 5 and 6, respectively while the 20 vol.% models used values of 3 for both fiber and cell aspect ratios. For volume fraction effects, the fiber and cell aspect ratios were both fixed at 3 and numerical results were carried out for volume fractions of 10%, 20% and 30%. For the fiber aspect ratio study, the fiber volume fraction was fixed at 30%; the fiber and cell aspect ratios were set equal to one another to eliminate spacing effects and numerical results carried out for values of 1, 3, 6 and 10. For the fiber spacing study, the fiber volume fraction was again fixed at 30%; the cell aspect ratio was fixed at 6 and numerical results were carried out for fiber aspect ratios of 3, 6 and 10.

Contours of von Mises effective stress were generated to determine the location of initial yielding in the matrix and the subsequent growth of the plastic zone due to loading. These models were developed using approximately twice the number of elements used in the constitutive response models to ensure clarity and resolution of the contour curves.

B. MATERIAL TESTING

The material testing portion of this study primarily focused on the tensile testing of both unreinforced and fiber-reinforced Al 6061 to extract mechanical properties for use in the numerical models , and in the case of the fiber-reinforced aluminum, to serve as

a comparison to assess the accuracy of the numerical predictions of stress-strain response. The composite material was procured from Advanced Composite Materials Corporation (ACMC), Greer, SC, and was produced using powder metallurgy (P/M) techniques. Extruded billets were subsequently produced from the P/M compacts for 20 vol.% SiC/Al 6061 at a reduction ratio of 11:1 and 30 vol.% SiC/Al 6061 at a reduction ratio of 6.5:1. The composite matrix was heat treated to the T6 condition by the manufacturer. Tensile test specimens with 1.0″ gage lengths were cut from the extruded stock such that the longitudinal axis of the sample was aligned with the extrusion direction. Unreinforced Al 6061-T6 tensile specimens were machined from plate stock.

The tensile specimens were mounted in a screw-driven Instron machine and pulled at rates of 1.0 mm/min for the aluminum samples and 0.127 mm/min for the composite samples. Clip-on extensometers were used to record engineering strain values during the test. The curves for the Al 6061 samples were used to determine values of yield strength and strain-hardening modulus for input into the numerical models. The value of the strain-hardening modulus was determined by fitting a curve from the offset yield point to the stress-strain curve within the expected strain range of the composite, in this case 5%. A more accurate value would be obtained by using an unreinforced powder sample from the same lot that the composite was produced, followed by heat treatment together with the composite samples to ensure uniformity in material processing.

An optical micrograph was obtained from a sample of the 30 vol.% extruded stock to determine average values of fiber aspect ratio and cell aspect ratio as well as to serve as a microstructural comparison when developing the unit cell models.

III. RESULTS AND DISCUSSION

A. COMPARISON OF ALIGNED AND STAGGERED FIBER MODELS

The sensitivity of composite constitutive response to imposed modeling constraint can be seen in Figure 3. As shown in Figure 3a, the unconstrained aligned-fiber model for a composite with 30 vol.% SiC whiskers of aspect ratio 5 predicts a Young's modulus (E) of 148 GPa, a proportional limit (PL) of 181 MPa and a yield strength (YS) of 276 MPa. The aligned-fiber model with constraint, in comparison, predicts the composite E, PL and YS values as 163 GPa, 292 MPa and 429 MPa, respectively. The constrained model also predicts a substantially higher work-hardening rate than the unconstrained model. Figure 3a also shows the experimental data for a 30 vol.% metal-matrix composite (MMC). By comparing analytical results with experimental data, it is evident that both the constrained and unconstrained models overestimate composite stiffness slightly. This can be attributed to the fact that the models assume perfectly aligned, parallel fibers. From Figure 1, the fibers in the experimental material are clearly neither aligned nor parallel. Additionally, some deviation is expected due to the mismatch between the fiber aspect ratio and fiber spacing assumed in the model and that occurring in the actual composite. The unconstrained model was found to underestimate the composite yield strength and work-hardening rate considerably. This is expected since the matrix in the unconstrained model is unable to "sense" the presence of adjacent unit cells and, therefore, is allowed to undergo relatively unconstrained plastic flow. The constrained model, on the other hand, is a much more realistic representation of an actual composite, although it predicts an appreciably higher yield strength and work-hardening rate. This, as discussed earlier, is attributable to the considerable deviation of the actual MMC from the idealized fiber configuration assumed in the model.

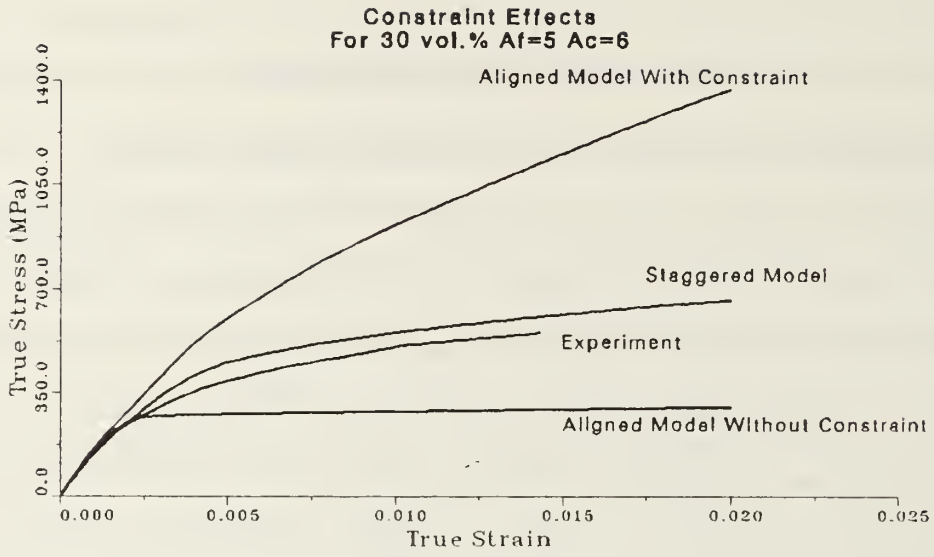

(a)

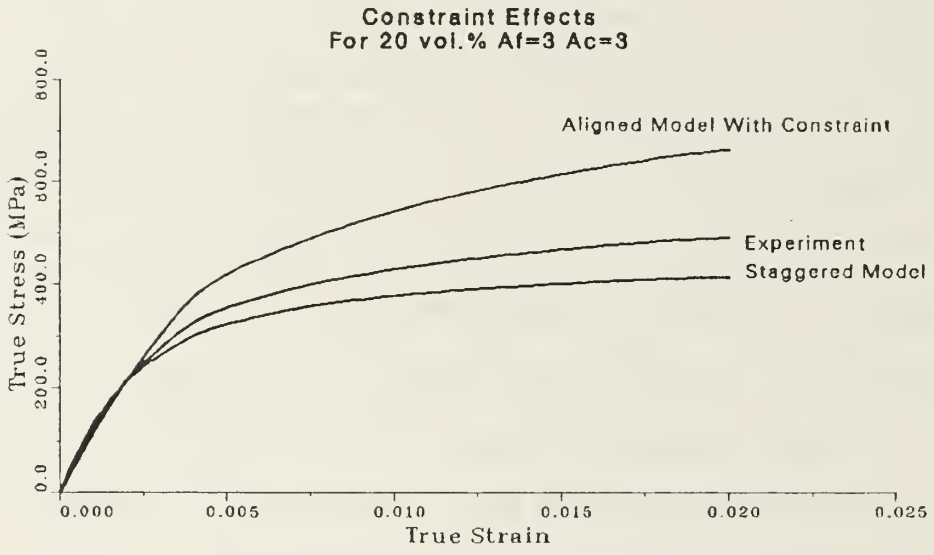

(b)

Figure 3. **Modeling Constraint Effects:** Comparison of aligned and staggered models with a (a) 30 vol.% tensile specimen and (b) 20 vol.% tensile specimen, respectively.

As seen in Figure 3a, the staggered model provides a closer approximation of the experimental data, despite the partially relaxed radial compatibility conditions (section II.A.2). The model predicts stiffness, proportional limit and work-hardening rate values which are reasonably close to the actual composite, but overestimates the yield strength.

The above discussion suggests that the degree of fiber alignment along the loading axis and the extent to which the adjacent fibers are shifted with respect to each other has as large effect on the accuracy of the analytical predictions. The degree of fiber alignment increases with increasing extrusion ratio, and hence it is expected that the agreement between analytical results and experimental data will improve with larger extrusion ratios. In the limiting case where the extrusion ratio is very high and all the fibers are perfectly aligned along the loading axis, the predictions of the aligned model are expected to match the experimental data reasonably well, although some over-prediction is likely since some degree of lateral misalignment is probable. In that case, the staggered fiber model is probably a more reasonable approximation, provided the radial boundary conditions of the model are adjusted appropriately. With the present radial boundary conditions, however, the staggered model is expected to somewhat underestimate the mechanical properties (PL,YS) of a composite with a very large extrusion ratio (i.e. a high degree of fiber axial alignment).

Figure 3b illustrates the effect of the imposed modeling constraints compared with 20 vol.% experimental data. Both aligned and staggered models give reasonable predictions of stiffness, with experimental values of proportional limit, yield strength and work-hardening rate lying between the values predicted by the numerical models. As expected, because of the higher extrusion ratio of the 20 vol.% sample (11:1, compared to 6.5:1 for the 30 vol.% sample), the predictions of the constrained aligned-fiber model are in closer agreement with the experimental data than at 30 vol.%. The staggered model now underpredicts the composite response somewhat due to the relaxed radial

compatibility condition. From the above, it is reasonable to assume that the aligned-fiber model is a fair approximation of a real composite provided the extrusion ratio is very large. The staggered model with the present boundary conditions, however, while yielding reasonable predictions for composites with low to medium extrusion ratios, is not a correct representation of the constraint mechanisms operative in an actual MMC. Hence, the aligned-fiber model was the model of choice for the parametric study presented in subsequent sections.

The close agreement between analytical results and experimental data at low fiber volume fractions is well represented in the literature [Refs. 18,19]. The majority of previous studies have made numerical comparisons with control systems of volume fractions from 5% to 20%. The greater level of error at higher volume fractions can be attributed to the modeling process; at high volume fractions, the reduced lateral and longitudinal spacing between the fiber and cell result in increased levels of matrix constraint, and hence have a significant effect on the plastic flow behavior of the material. Hence a slight error in the estimation of fiber aspect ratio and fiber spacing translates into a large error in the prediction of composite response. For low volume fraction models, the boundaries of the unit cell are relatively free of these constraint effects and the numerical results more closely represent experimental results.

Another factor affecting the trend of the numerical results is the difference in mean fiber aspect ratio between the 20 and 30 vol.% samples. The 20 vol.% sample was processed at a reduction ratio of 11:1, whereas the 30 vol.% sample was processed at a ratio of 6.5:1. The end result of this difference is that the 20 vol.% sample experiences more fiber breakage during processing and subsequently exhibits a lower value of average fiber aspect ratio ($A_f = 3$) than the 30 V% sample ($A_f = 5$). Christman *et al.* [Ref. 18] observed that the use of particulate-reinforced models ($A_f = 1$) produced better agreement with experimental data than using whisker-reinforced systems. The reasons

for increased accuracy of the numerical models were (1) particulate misalignment with the tensile axis had a negligible effect on composite response for $A_f = 1$, (2) the particulate morphology produced less plastic flow constraint in the composite with the result that the idealized cell model more closely emulated the behavior of the actual material and (3) clustering effects in particulate-reinforced composites had less of an effect on the stress-strain response than in whisker-reinforced materials.

B. EFFECT OF FIBER VOLUME FRACTION

Figure 4 illustrates the effect of increasing volume fraction on the constitutive response of the composite. The numerical models predict the experimentally observed trends of increasing values of stiffness, yield strength and work-hardening rate with increasing volume fraction. The primary mechanisms affecting composite behavior in this case are increased plastic flow constraint, increased dislocation density and enhanced matrix-to-fiber load transfer with increasing reinforcement volume fraction. Christman *et al.* [Ref. 18] observed that as volume fraction increased, the magnitude of the hydrostatic stresses in the matrix dramatically increased producing greater resistance to plastic flow, and hence higher work-hardening rates. Another trend predicted by the models is the experimentally observed behavior of decreasing and subsequent increasing values of proportional limit with increasing volume fraction. Levy and Papazian [Ref. 21] reported this effect as a function of localized stress concentrations in the matrix at low levels of reinforcement addition.

C. EFFECT OF FIBER ASPECT RATIO

The dependence of composite constitutive response on fiber aspect ratio can be seen in Figure 5. The numerical results predict an increase in stiffness, proportional limit, yield strength and work-hardening rate with increasing aspect ratio. Additionally, the curves indicate that the strengthening effect becomes less pronounced as the fiber aspect ratio increases. The increased strength of composites with larger aspect ratios can be

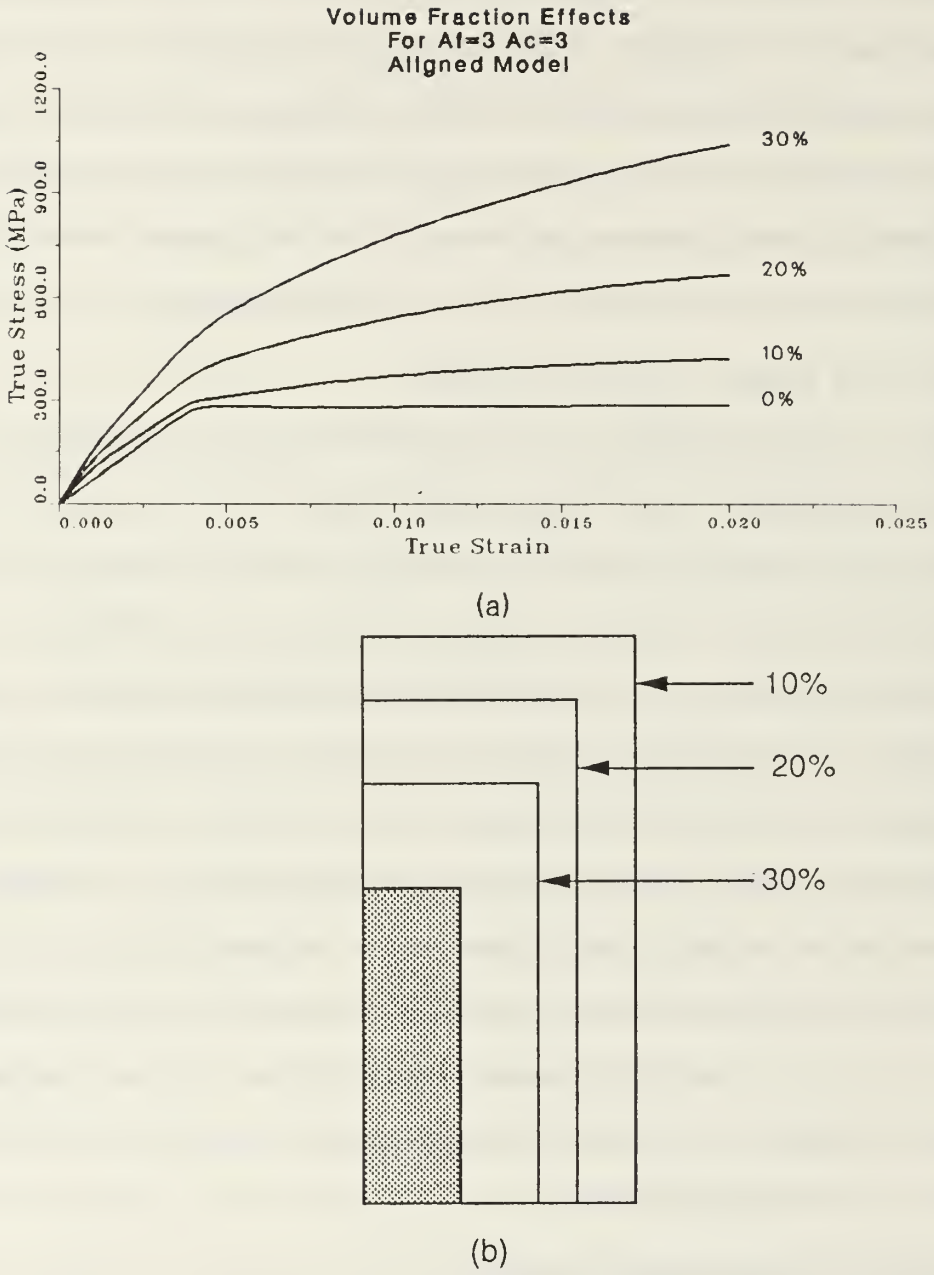

Figure 4. **Volume Fraction Effects:** (a) Curves of predicted composite response for reinforcement volume fractions of 0%, 10%, 20% and 30%, respectively and (b) schematic of model configurations.

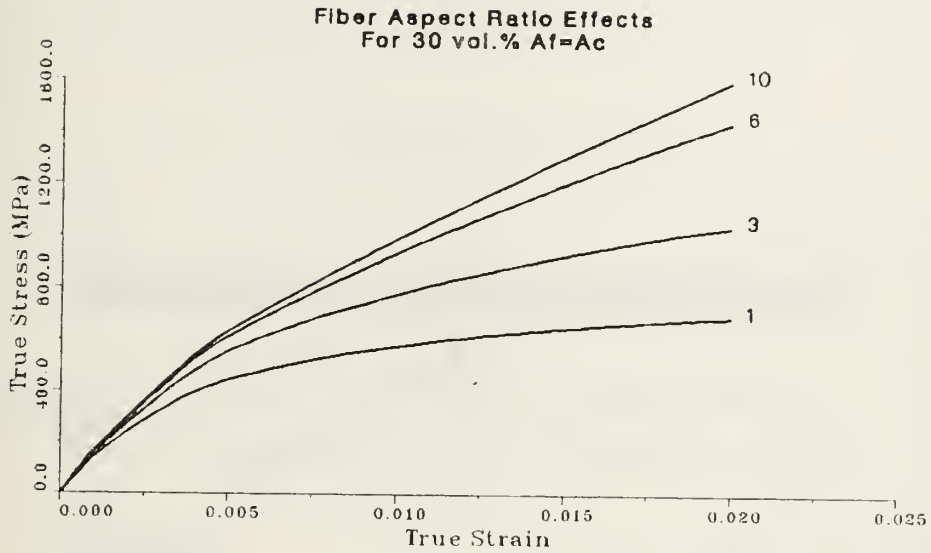

(a)

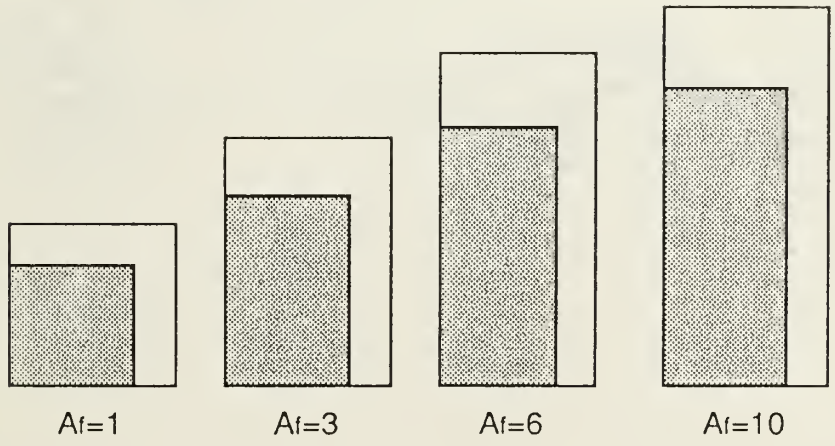

(b)

Figure 5. **Fiber Aspect Ratio Effects:** Curves of composite response for fiber aspect ratios of 1,3,6 and 10, respectively.

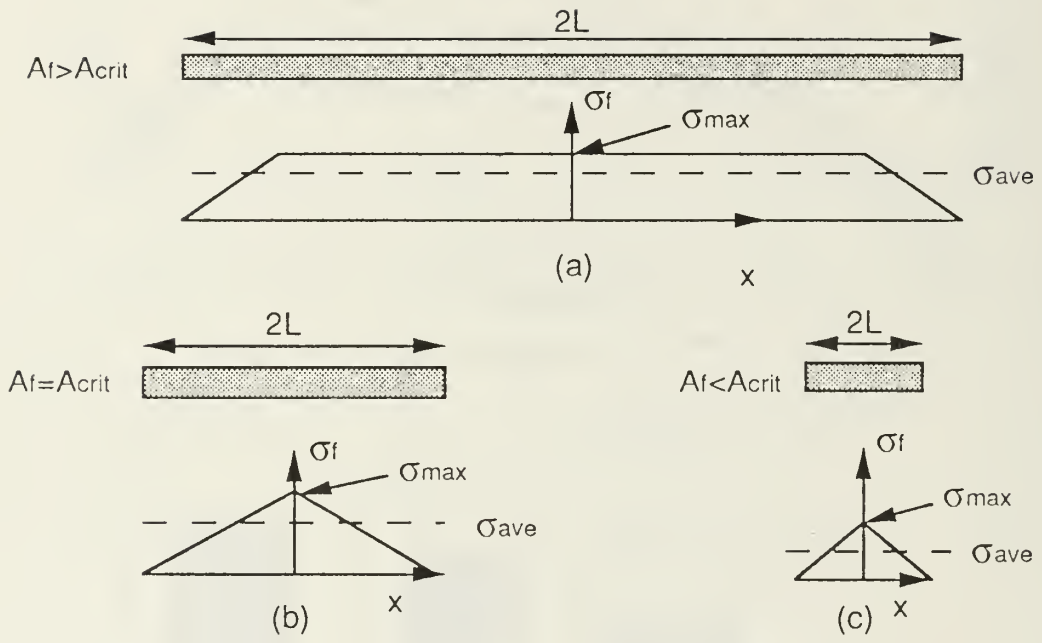

Figure 6. **Effect of the Critical Fiber Aspect Ratio:** Schematic representation of the maximum and average stresses built up in the fiber for the cases of (a) $A_f > A_{crit}$, (b) $A_f = A_{crit}$ and (c) $A_f < A_{crit}$.

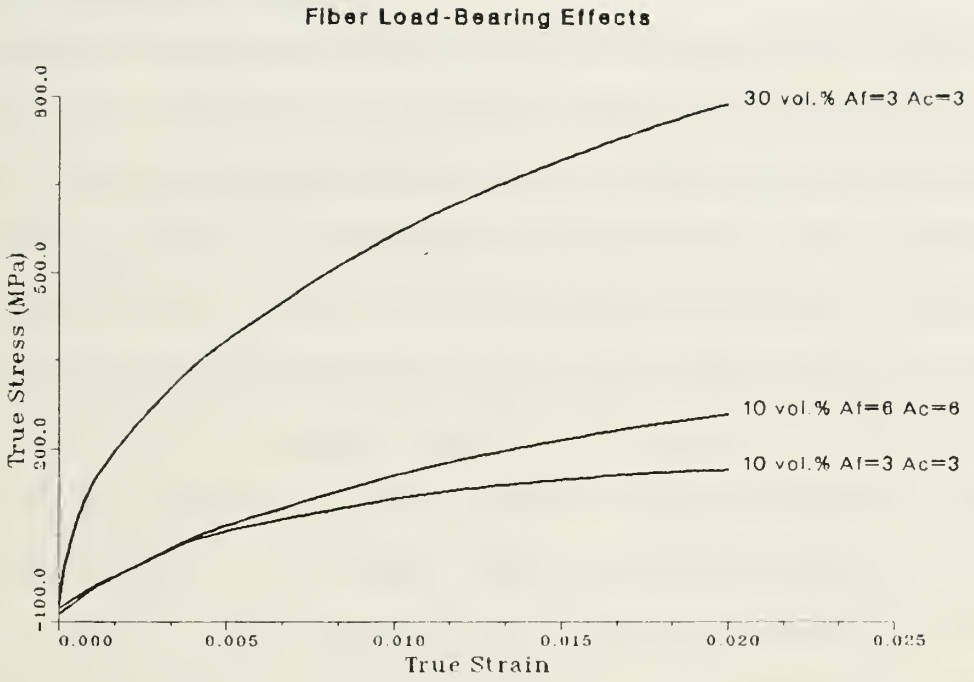

Figure 7. Fiber Load-Bearing Behavior: Effects of fiber aspect ratio and volume fraction on the load-bearing ability of the fiber in the presence of residual stresses.

attributed to increased load transfer between the matrix and the longer fibers. Piggott [Ref. 27] described this strengthening effect in terms of a critical aspect ratio (A_{crit}), below which the load transfer between the matrix and fiber fail to produce the maximum fiber axial stress possible. Figure 6 illustrates this effect. For fiber aspect ratios above the critical value, surface shear transfer from the matrix can result in maximum load transfer to the fiber. For aspect ratios equal to the critical value, portions of the fiber can still experience maximum load transfer, although the average stress in the fiber is lower. When the aspect ratio is reduced to below the critical value, the load transfer is such that the resulting values of axial stress and average stress in the fiber are far below the previous cases. In this case, the relative inability of the matrix to transfer load to the fiber results in the matrix bearing a substantially greater portion of the applied load, leading to lower values of composite stiffness, yield strength and work-hardening rate. It is generally believed that matrix-to-fiber load transfer is not a major strengthening mechanism in discontinuously-reinforced MMC's [Refs. 28 ,29], which are thought to be strengthened primarily by increased matrix dislocation density. However, as shown in Figure 7, the average axial stress supported by the fiber increases with both increasing fiber volume fraction and fiber aspect ratio. It is evident that load transfer from the matrix to the fiber is an important factor in the strengthening of fiber-reinforced MMC's. This is further supported by the increase in Young's modulus observed both analytically and experimentally with increasing fiber volume fraction. If an increased dislocation density were the only strengthening mechanism, no increase in stiffness would be observed on increasing the reinforcement content of the composite.

The reduced degree of additional strengthening with increasing aspect ratio at higher values of fiber aspect ratio is observed only for aligned fibers. The trends observed in other studies [Refs. 19,21] using the staggered-fiber arrangement indicate that the level of strengthening in the composite increases with increasing aspect ratio. This is contrary

to the trend observed in the aligned-fiber model. One explanation of the difference in behavior is due to the effect of fiber overlap in the staggered model. As fiber aspect ratio increases, the degree of fiber overlap increases producing greater geometric constraint and therefore increased resistance to plastic flow.

D. EFFECT OF FIBER SPACING

The sensitivity of composite constitutive response to variations in fiber spacing is shown in Figure 8a. The results indicate that changes in fiber spacing have little effect on composite elastic properties; however, the resistance to plastic flow in the material is significantly affected by close end-to-end and side-to-side fiber spacing. The curve representing close end-to-end spacing ($A_c = 3$) exhibits the greatest increase in work-hardening rate due to the relatively small amount of matrix material separating adjacent fiber ends. This results in a substantial increase in load transfer across the fiber end surface, and hence increased resistance to plastic flow. The curve representing close side-to-side fiber spacing ($A_c = 10$) exhibits a somewhat lower work-hardening rate than observed in the close end-to-end spacing case. The lateral constraint imposed on the composite in this case, while not as great an effect as for $A_c = 3$, still increases the resistance to plastic flow in the material above that of the composite model without spacing constraints ($A_c = 6$).

E. EFFECT OF THERMAL RESIDUAL STRESSES

The primary aim of this study has been to assess the role of thermal residual stresses on the stress-strain behavior of metal-matrix composites. The results contained in this section describe this effect in terms of fiber volume fraction and geometric constraint due to the modeling of fiber arrangement. In addition, load-bearing characteristics of the fiber during deformation is studied in an effort to more fully explain the stress-strain behavior of the numerical models.

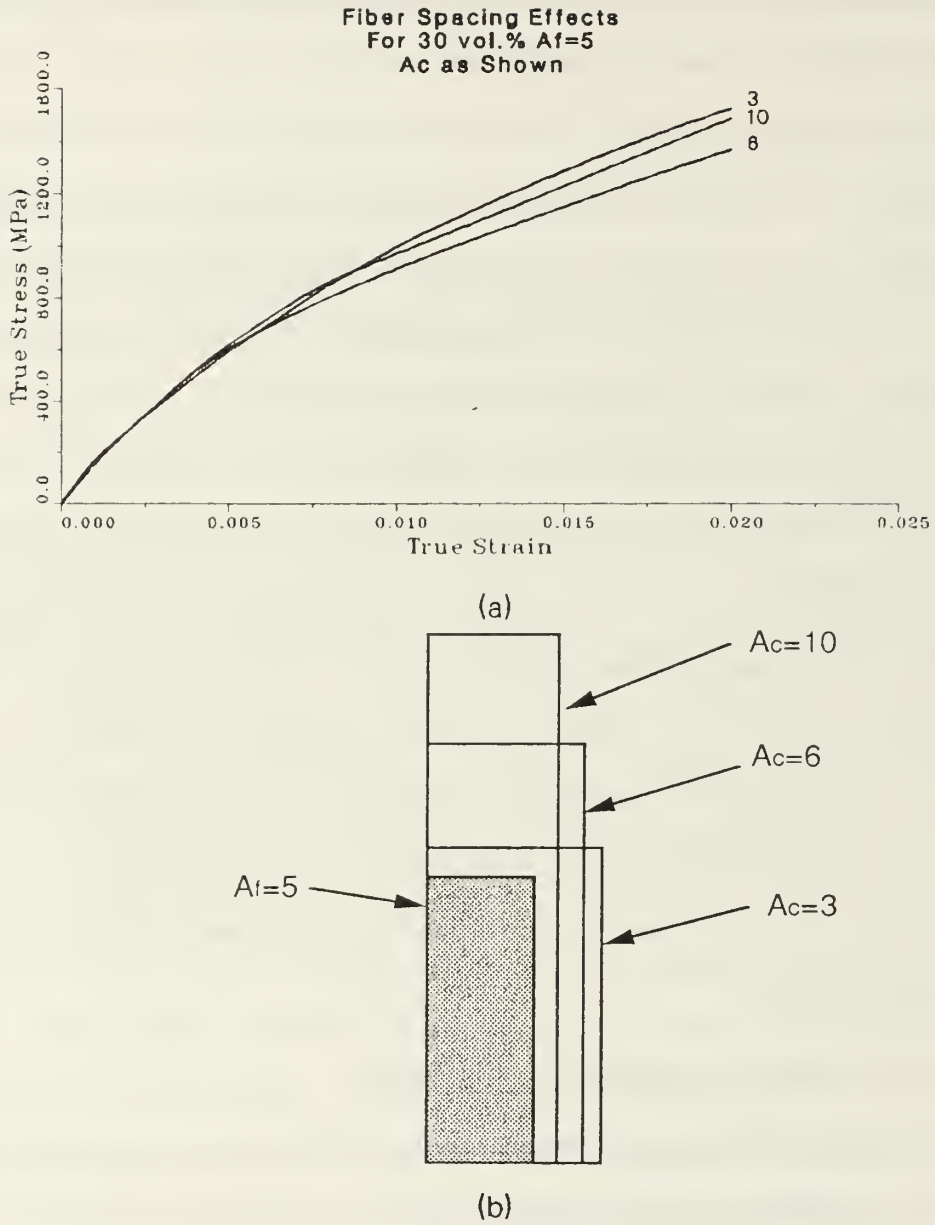

Figure 8. Fiber Spacing Effects: (a) Numerical results for fixed volume fraction and fiber aspect ratio with variable fiber spacing and (b) schematic of fiber spacing models.

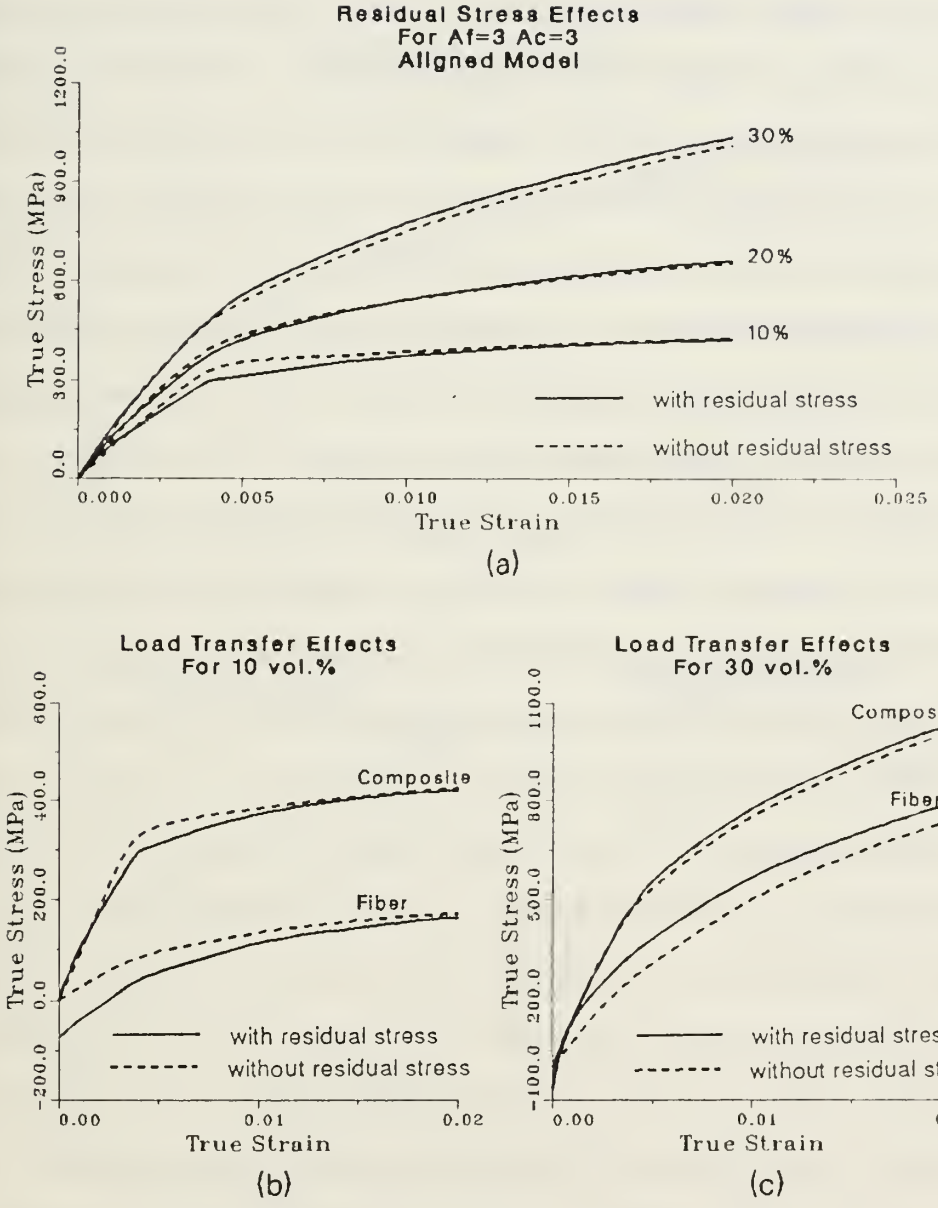

Figure 9. Residual Stress and Volume Fraction Effects: Effects of residual stress as a function of (a) volume fraction. Also shown are the stresses supported by the fiber as a function of strain for (b) 10 vol.% and (c) 30 vol.%.

dual stress predicts a higher composite stiffness and yield strength, while the model with residual stress exhibits a higher work-hardening rate. The results for 30 vol.% indicate that both curves exhibit similar behavior in the elastic regime, however the curve with residual stress displays a slightly higher work-hardening rate. To explain these results, plots of fiber stress-versus-strain were compared with the corresponding composite curves. The results indicate that for 10 vol.% the presence of residual stresses inhibits the load transfer to the fiber resulting in an overall decrease in composite strength in both the elastic and plastic regimes. The results for 30 vol.% indicate the opposite trend. The presence of residual stresses enhances the transfer of load to the fiber enabling the composite as a whole to exhibit greater strength properties. From Figure 9, it is also evident that the rate of load transfer to the fiber with increasing strain is much higher in the 30 vol.% composite. While for the 10 vol.% composite, the rate of load transfer with and without residual stresses is fairly close, the 30 vol.% exhibits a much higher rate initially in the presence of residual stresses, leading to the observed cross-over of the fiber stress-strain curves. This effect indicates that for the 30 vol.% composite, the presence of residual stresses produces a much higher rate of load transfer from the matrix to the fiber resulting in the observed increase in composite mechanical properties.

Figure 10 illustrates the role of thermal residual stresses as a function of imposed geometric constraint. In this case, the aligned and staggered models are compared at a volume fraction of 30% and equal cell and fiber aspect ratios of 3. The results indicate that the aligned model with residual stress predicts greater strengthening effects in both the elastic and plastic regimes, whereas the staggered model exhibits lower stiffness and yield strength and a higher work-hardening rate in the presence of residual stresses. The fiber stress-strain results for the staggered model indicate that the transfer of load from the matrix to the fiber is inhibited in the presence of residual stresses, similar to the results for the aligned model at 10 vol.% (Figure 9b).

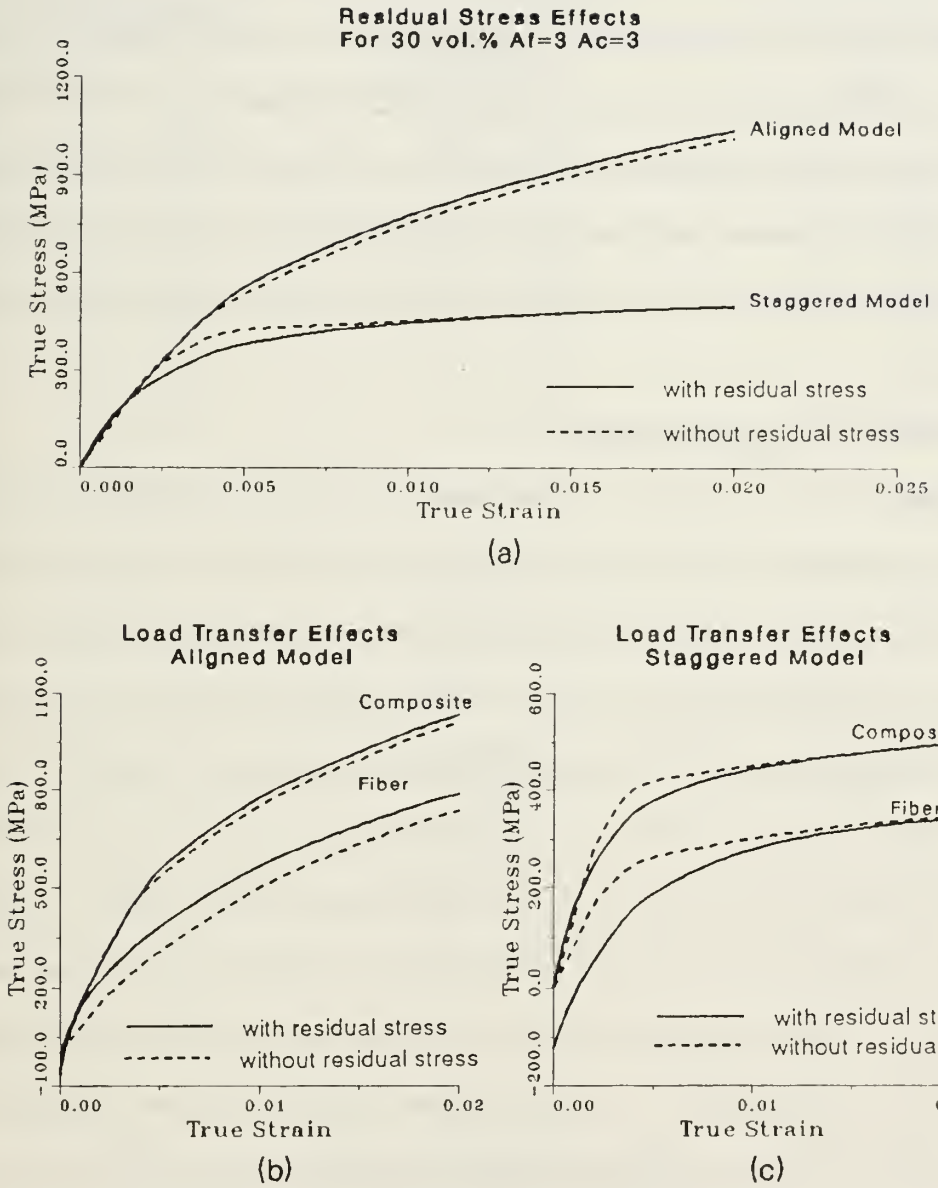

Figure 10. **Residual Stress and Modeling Constraint Effects:** Effects of residual stress as a function of (a) geometric constraint. Curves of fiber stress-strain response for a (b) 30 vol.% aligned and (c) 30 vol.% staggered model.

F. PLASTIC ZONE INITIATION AND GROWTH

In the previous section, the role of thermal residual stresses as functions of volume fraction and modeling constraint were discussed in terms of their effect on the overall stress-strain response of the composite. In this section, the role of residual stresses on the initiation and growth of the plastic zone during thermal and subsequent tensile loading of the composite is studied with reference to the effect of reinforcement volume fraction, modeling constraint and fiber spacing on the effective stress state in the composite in an effort to identify the main deformation characteristics operative in an actual composite.

1. Thermal Residual Stress Effects

Figure 11 shows a 30 vol.% aligned model at selected stages of deformation. The contours of residual effective stress ($\varepsilon = 0$) reveal that a plastically deformed zone ($\sigma_{eff} > 275$ MPa) exists along the entire fiber-matrix interface with the highest stress states occurring along the fiber corner. The plot also indicates that the entire area of the matrix from the lateral interface to the cell boundary has undergone plastic deformation. The stress levels in the fiber indicate a compressive stress zone in excess of 500 MPa concentrated along the fiber corner and extending along the end surface. This high stress zone quickly dissipates to below 250 MPa a short distance from the end surface of the fiber. At $\varepsilon = 0.001$, the plastic zone along the lateral surface of the interface begins to expand in the radial direction. The matrix region adjacent to the end of the fiber experiences a stress relaxation as load is transferred from the matrix to the fiber across the fiber tip and end surface. This effect can be seen in the growth of the region of the fiber tip stresses above 500 MPa,indicative of the fiber bearing a greater portion of the applied loading at $\varepsilon = 0.001$. At $\varepsilon = 0.0045$, the entire fiber is stressed above 500 MPa and the plastic zone has further developed in the area between the lateral interface and cell

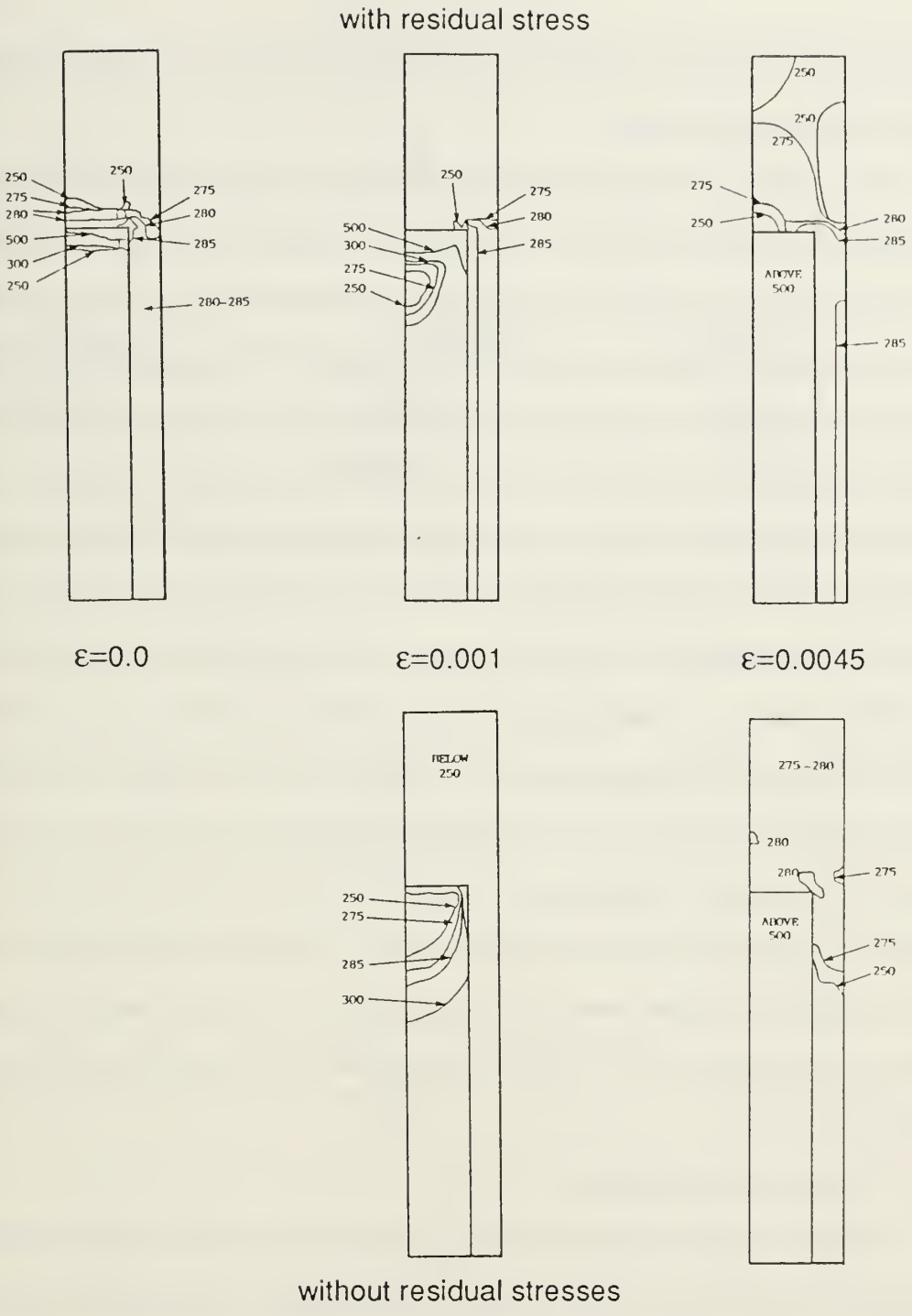

Figure 11. Plastic Zone Development-Residual Stress Effects: Contours of effective stress for a 30 vol.% aligned model with $A_f = A_c = 6$.

boundary and has begun to expand to the matrix region above the fiber as evidenced by the 275 MPa contour lines.

The contours for the 30 vol.% model without residual stresses illustrates the fundamental difference in behavior of the composite with and without residual stresses. In the model without residual stress, plastic deformation begins in the matrix region above the fiber and at the fiber corner. At increased load levels, the plastic zone expands in the axial direction into the matrix material above the fiber, followed by radial growth along the lateral fiber interface out to the cell boundary. Thus, when residual stresses are absent, the matrix region next to the lateral (cylindrical) fiber surface is the last to deform plastically, suggesting that the matrix in this region is able to transfer a large portion of the applied load to the fiber. Little, if any, load transfer occurs across the fiber ends in this case. When thermal residual stresses are present, on the other hand, the fibers are in axial compression prior to loading, and a large degree of load transfer takes place across the fiber ends, as evidenced by the initial stress relaxation in the matrix and the subsequent development of a small plastic zone upon external loading. The increased load transfer across the fiber end surface, however, is at the expense of somewhat reduced load transfer across the lateral portion of the fiber-matrix interface, as evidenced by the increase in the effective stress in the plastic zone adjacent to the interface from the outset.

2. Volume Fraction Effects

Figure 12 shows contours of effective stress for a 10 vol.% aligned model. The results clearly illustrate the effect of varying reinforcement volume fraction on the deformation characteristics of the composite. The absence of fiber spacing constraints in the 10 vol.% numerical model results in a residual stress field in the matrix characterized by larger levels of plastic deformation in the vicinity of the fiber-matrix interface than for the 30 vol.% model. The fiber exhibits an extremely high compressive residual stress

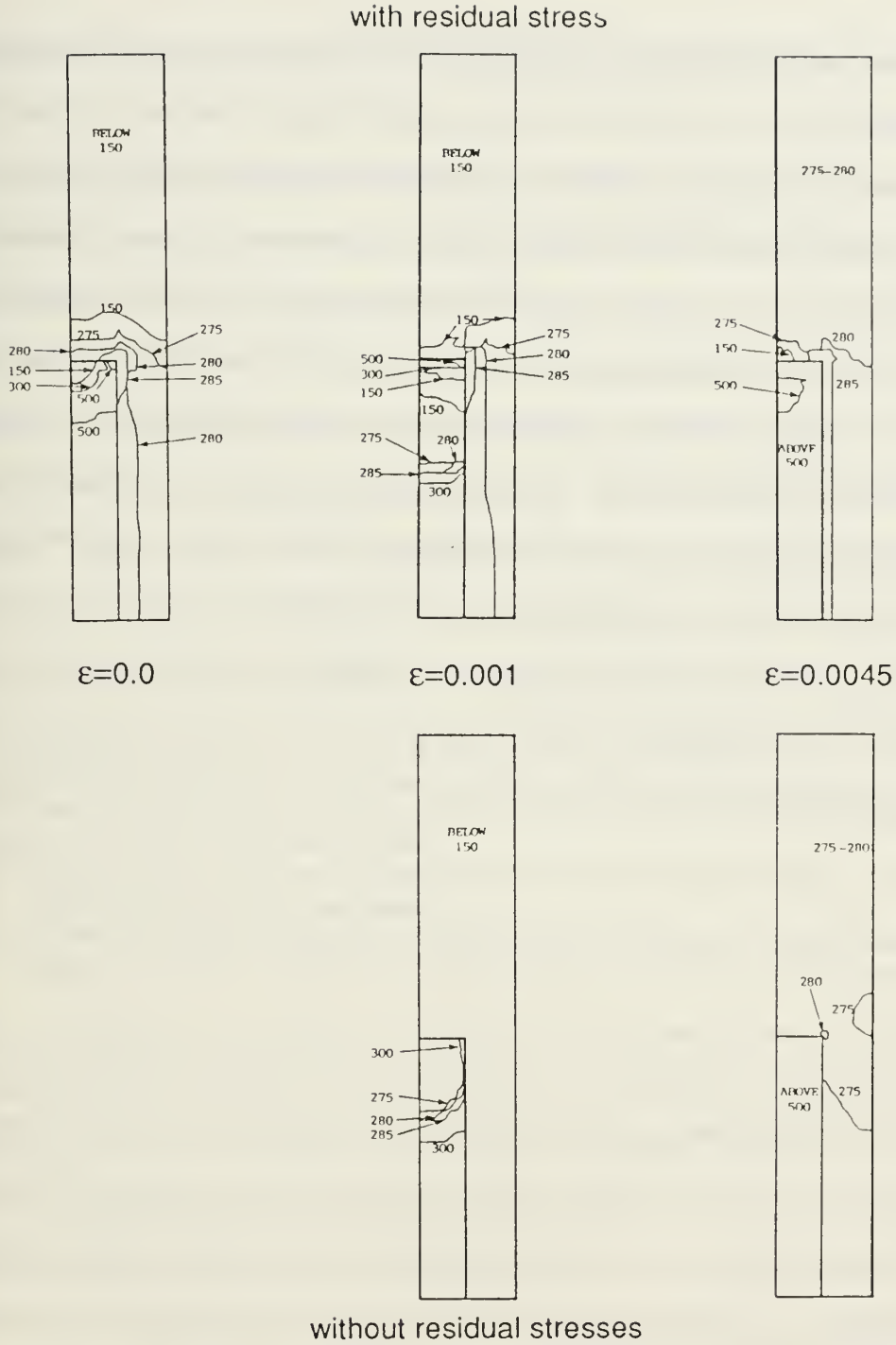

Figure 12. **Plastic Zone Development-Volume Fraction Effects:** Contours of effective for a 10 vol.% aligned model with $A_f = A_c = 6$.

characterized by a 500 MPa zone in the vicinity of the fiber corner, a low stress region in the material below the end surface and an adjacent high stress region (above 500 MPa) extending to the midpoint of the fiber. This is contrasted with the 30 vol.% model in which the region below the top surface of the fiber is relatively unstressed (below 250 MPa). Physically, the 10 vol.% model has a larger volume of matrix material surrounding the fiber which, upon quenching, encounters less restriction in movement than in the 30 vol.% model. The matrix, therefore, is free to deform plastically to a greater extent in the vicinity of the interface. The smaller end surface area of the fiber precludes the level of load transfer across this surface exhibited in the 30 vol.% model. The end surface of the fiber fails to accommodate the stress build-up in the matrix in this region resulting in increased levels of matrix plasticity. The extent of matrix material above the fiber in the 10 vol.% model, being greater than in the 30 vol.% model, implies that for a given applied strain, the matrix in the 10 vol.% model must transfer the subsequent displacements a greater distance prior to encountering the fiber. This results in lower levels of load transfer, and hence lower levels of composite strength in the 10 vol.% model.

At low levels of applied strain ($\varepsilon = 0.001$), the matrix material adjacent to the top surface of the fiber experiences a stress relaxation as the fiber accommodates the applied load. During this stage, the plastic zone grows only slightly as the majority of the load is transferred to the fiber. At $\varepsilon = 0.0045$, the plastic zone experiences both radial and axial growth with the greatest expansion occurring in the radial direction as in the 30 vol.% model. The matrix in the region well above the fiber interface exhibits a uniform stress state of 275 to 280 MPa. Noteworthy is the lack of high and low stress zones evident in the matrix region above the fiber in the 30 vol.% model. In the 30 vol.% material, these zones presumably result from increased levels of matrix hydrostatic stress

due to the higher volume of reinforcement, although this premise has not been investigated.

The 10 vol.% model in the absence of residual stresses exhibits the same axial growth of the plastic zone as in the 30 vol.% model. The fiber in this case, however, accommodates a greater level of load transfer from the matrix than with residual stresses present. This provides one explanation of the results presented in Figure 9 (i.e. the decrease in yield strength due to the presence of residual stresses in the 10 vol.% MMC versus the increase in yield strength observed in the 30 vol.% MMC in the presence of residual stresses). In the 10 vol.% composite, the degree of load transfer across the fiber ends in the presence of residual stresses is much less than in the 30 vol.% composite. Hence, while the presence of residual stresses yields greater composite strength in the 30 vol.% model, it reduces the strength in the 10 vol.% composite since the decrease in load transfer across the lateral fiber surface is not offset by a corresponding increase in load transfer across the fiber end surface.

3. Effects of Modeling Constraints

Figure 13 shows contours of effective stress for a 30 vol.% staggered fiber model. The premise for studying the staggered fiber arrangement was the expectation that significant stress states would be developed in the matrix in the region between overlapping fiber ends, resulting in an important deformation mechanism operative in an actual composite material. A comparison of Figure 11 and Figure 13 reveals a profoundly different pattern of plastic zone development. The plot of residual effective stress reveals a complicated deformation pattern composed of (1) plastic zones adjacent to the fiber interface of larger magnitude than existing in the 30 vol.% aligned model, (2) larger levels of plastic deformation in the matrix region between the lateral fiber interface and the cell boundary and (3) regions of plastic deformation in the matrix well away from the fiber interface that is a result of the boundary conditions imposed on the

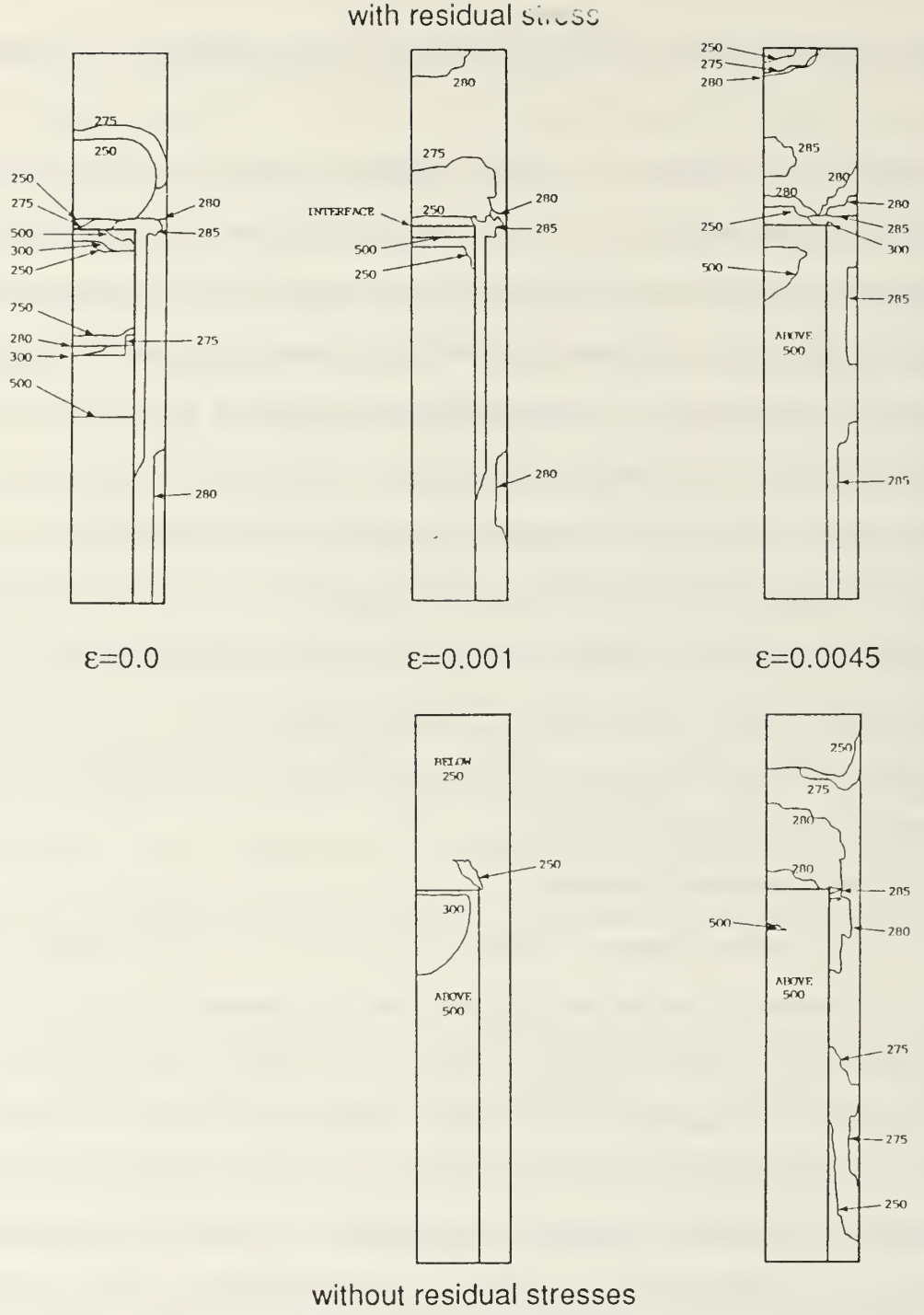

Figure 13. Plastic Zone Development-Constraint Effects: Contours of effective stress for a 30 vol.% staggered model with $A_f = A_c = 6$.

numerical model for the staggered fiber arrangement. A fundamental deformation characteristic of this model in the presence of residual stresses is the growth of the plastic zone in the matrix region above the interface first before the radial growth common in the aligned models occurs. At higher strain levels ($\varepsilon = 0.0045$), the plastic regions intersect followed by gross plasticity in the matrix.

The contour plots of the staggered model without residual stresses exhibits the axial growth of the plastic zone common in the aligned models. The load transfer to the fiber occurs more readily in this case than in either the staggered model with residual stress or the 30 vol.% aligned model. This factor accounts for the observed increase in yield strength and stiffness over the same model with residual stresses present (Figure 10a). The observed increase in work-hardening rate in the staggered model with residual stresses can be attributed to the development of hydrostatic stress pockets in the matrix [Ref. 21] along the cell boundary that offer an increased resistance to plastic flow over the model without residual stresses.

4. Fiber Spacing Effects

Figure 14 illustrates the effect of fiber spacing in the presence of residual stresses on the development and growth of plastic deformation in the composite matrix. The results indicate that side-to-side fiber spacing has the greatest impact on the level of residual stress in the matrix as shown in Figure 14a. The plastic zone for this model extends throughout the entire matrix with the highest stress levels occurring at the interface. In contrast, the models with $A_f = 6$ and 10, respectively exhibit a plastic zone confined to the region near the fiber interface. Figure 14c shows the stress distributions in the composite with close end-to-end spacing. The resulting deformation pattern reveals a plastic zone with larger radial extent than the $A_f = 6$ model due to the increased lateral spacing. The plastic zone on the top surface of the fiber is confined to a relatively thin layer of material with an adjacent low-stress zone in the material at the

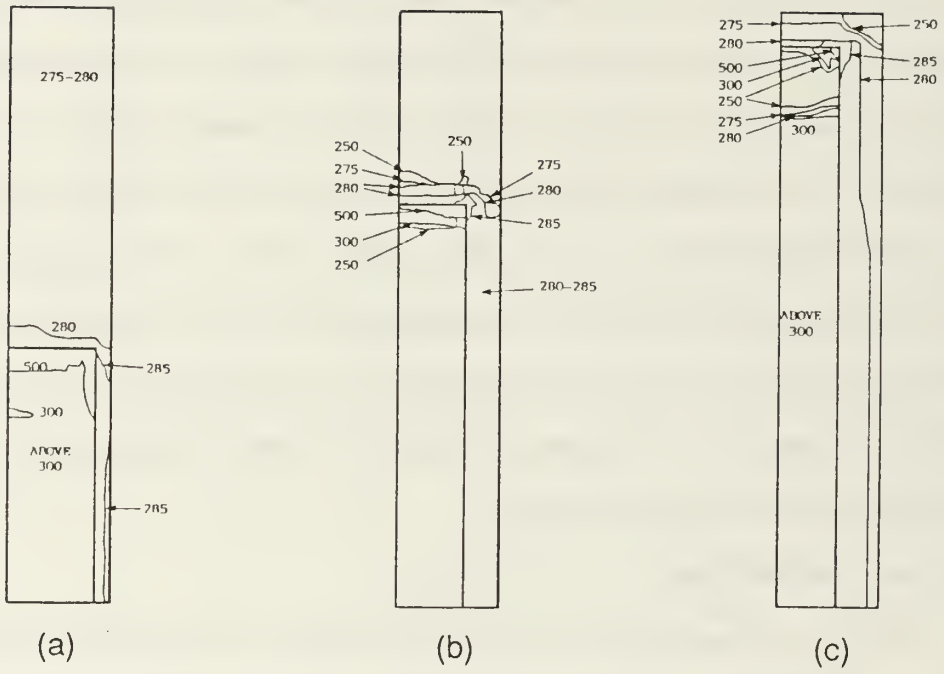

Figure 14. Plastic Zone Development-Fiber Spacing Effects: Contours of effective stress for 30 vol.% aligned fiber models with cell aspect ratios of 6 and fiber aspect ratios of (a) 3, (b) 6 and (c) 10, respectively.

relatively thin layer of material with an adjacent low-stress zone in the material at the top of the cell. The stress states in the fiber are a maximum in the $A_f = 3$ model followed by the $A_f = 6$ and 10 models, respectively. These results help explain the stress-strain behavior observed in Figure 8. Even though the material with close side-to-side spacing initially exhibits greater levels of plastic deformation throughout the matrix, the close proximity of adjacent fiber end surfaces produces a more pronounced effect on the composite work-hardening rate.

IV. CONCLUSIONS

In this study, the uniaxial stress-strain response of an SiC_w/Al 6061 composite was investigated to assess the role of thermal residual stresses on the constitutive behavior of the material. The following summarize the relevant findings:

1. Elastic-plastic and thermo-elastic-plastic analysis using finite-element models of fiber-reinforced metal-matrix composites can be used to predict uniaxial stress-strain behavior given the thermo-mechanical properties of the constituent phases as a starting point.
2. Aligned and staggered fiber models are both necessary to describe the fundamental deformation mechanisms operative in the composite material.
3. The stiffness, yield strength and work-hardening rate of the composite increase with increasing fiber volume fraction and fiber aspect ratio.
4. Variations in fiber spacing have little effect on composite elastic properties, but significantly affect the work-hardening rate for close side-to-side and end-to-end spacing.
5. The presence of residual stresses significantly impact the stress-strain behavior of the composite, principally by affecting the load transfer characteristics between the matrix and fiber.
6. The presence of residual stresses affect the initiation and continuation of plastic deformation in the matrix by producing a plastic zone adjacent to the fiber-matrix interface that, in general, expands radially outward from the lateral surface of the fiber to the cell boundary as loading increases. The absence of residual stress, in contrast, results in the simultaneous development of plastic zones in the matrix above the fiber end and along the fiber corner that expand axially as load increases.
7. The lateral spacing of adjacent fibers is an important factor affecting the magnitude and distribution of residual stresses in the composite.

APPENDIX A. SAMPLE ADINA INPUT FILE

```
* THIS INPUT FILE SIMULATES THERMAL AND TENSILE LOADING OF A
* METAL-MATRIX COMPOSITE.  THE PROGRAM INCLUDES COMMENTS AT
* APPROPRIATE LOCATIONS TO ILLUSTRATE SOME OF THE IMPORTANT
* FEATURES OF ADINA IN NON-LINEAR ANALYSIS.
*
* THE FOLLOWING BLOCK OF CODE CONTAINS ADINA CONTROL INFORMATION
DATABASE CREATE
CONTROL ORIGIN=UPPERLEFT PLOTUNIT=CM
FILEUNITS LIST=6 LOG=6 ECHO=6
*
* THE FOLLOWING BLOCK OF CODE CONTAINS SPECIFICATIONS FOR MODEL DEGREES OF
* FREEDOM, SOLUTION TIME PERIOD LENGTH AND TIME-STEP SIZE.  THE FIRST
* "MASTER" COMMAND LINE IS USED IN ELASTOPLASTIC ANALYSIS; THE SECOND
* COMMAND SIMULATES THE QUENCH PROCESS AND THE THIRD SIMULATES THE
* TENSILE LOADING FOLLOWING THE QUENCH.
* CAN BE USED IN DURING A GIVEN RUN, THE OTHER MUST BE COMMENTED OUT USING
* A '*'.
MASTER IDOF=100111 ITP56=0 NSTEP=6 DT=1.0
*MASTER IDOF=100111 ITP56=2 NSTEP=1 DT=1.0
*MASTER IDOF=100111 ITP56=2 NSTEP=6 DT=1.0
*
* THE FOLLOWING BLOCK OF CODE CONTAINS THE KINEMATIC AND ITERATION METHOD
* SPECIFICATIONS.  AUTOMATIC-ATS IS A FEATURE USED IN NON-LINEAR ANALYSIS
* TO ASSIST IN ACHIEVING THE REQUIRED TOLERANCE FOR THE OUT-OF-BALANCE
* ENERGY NORM.
KINEMATICS DISP=LARGE STRAINS=LARGE
ITERATION METHOD=FULL-NEWTON LINE-SEARCH=YES
AUTOMATIC-ATS N=10
*
* THE FOLLOWING COMMANDS RELATE TO THE PROGRAM OUTPUT.  COMMENT IN THE
* "WORKSTATION" COMMAND IF A HARDCOPY OF THE MODEL CONFIGURATION IS
* DESIRED.
HEADING 'VF=30% AF=3 AC=3'
PRINTOUT VOLUME=MAX
PORTHOLE FORMATTED=YES FILE=60
*WORKSTATION SYSTEM=4 DEVICE=0 OPTION=0
*
* THE FOLLOWING CODE SPECIFIES THE NATURE OF THE APPLIED TEMPERATURE LOAD.
* NUMBERS TO THE LEFT ARE TIME VALUES AND THE NUMBERS TO THE RIGHT ARE THE
* VALUES OF TEMPERATURE CHANGE FROM THE INITIAL TEMPERATURE OF THE MODEL.
TIMEFUNCTION 1
  0.0        0.0
  1.0     -505.0
*
* THE FOLLOWING TIME FUNCTIONS REPRESENT THE DISPLACEMENT LOADING SEQUENCE
* THE NUMBERS TO THE RIGHT ARE DISPLACEMENTS FROM THE REFERENCE LENGTH OF
* THE MODEL THAT CORRESPOND TO A GIVEN LOGARITHMIC STRAIN TO BE USED IN
* THE STRESS-STRAIN CURVE.  NOTE: THE DISPLACEMENTS FOR THE MODEL WITH
* RESIDUAL STRESSES START AT TIME=2.0 SINCE THE QUENCH PROCESS OCCURRED
* FROM TIME 0 to 1.0.  IN ADDITION, THE DISPLACEMENTS ARE INITIALLY
* NEGATIVE DUE TO THE QUENCH PROCESS.  THE SUBSEQUENT DISPLACEMENTS
```

```
* ARE ADDED TO THE NEW REFERENCE.  THE DISPLACEMENT SPECIFICATIONS
* IN ADINA ARE ALWAYS ABSOLUTE DISPLACEMENTS, MEANING THAT A RELATIVE
* CHANGE IN DISPLACEMENT CANNOT BE INPUT.
TIMEFUNCTION 2
* DISPLACEMENTS FOR ALIGNED MODEL WITH RESIDUAL STRESSES
  0.0        0.0
  2.0        -.015496
  3.0        -.013248
  4.0        -.00875
  5.0        0.00702
  6.0        0.01124
  7.0        0.06154
*
TIMEFUNCTION 3
* DISPLACEMENTS FOR ALIGNED MODEL WITHOUT RESIDUAL STRESSES
  0.0        0.0
  1.0        0.00448
  2.0        0.00897
  3.0        0.01796
  4.0        0.03598
  5.0        0.04502
  6.0        0.0905
*
* THE FOLLOWING BLOCK OF CODE INPUTS THE NODAL COORDINATES AND SPECIFIES
* THE NUMBER OF ELEMENTS DESIRED BETWEEN NODES.
SYSTEM 1 TYPE=CARTESIAN
COORDINATES
   ENTRIES     NODE      Y       Z
                 1       1.49    4.48
                 2       1.0     4.48
                 3       0.0     4.48
                 4       1.49    3.0
                 5       1.0     3.0
                 6       0.0     3.0
                 7       1.49    2.24
                 8       1.0     2.24
                 9       0.0     2.24
                10       1.49    0.0
                11       1.0     0.0
                12       0.0     0.0
*
LINE STRAIGHT 1 2  EL=3
LINE STRAIGHT 2 3  EL=6
LINE STRAIGHT 4 5  EL=3
LINE STRAIGHT 5 6  EL=6
LINE STRAIGHT 7 8  EL=3
LINE STRAIGHT 8 9  EL=6
LINE STRAIGHT 10 11 EL=3
LINE STRAIGHT 11 12 EL=6
*
LINE STRAIGHT 1 4  EL=9
LINE STRAIGHT 4 7  EL=5
LINE STRAIGHT 7 10 EL=14
LINE STRAIGHT 2 5  EL=9
LINE STRAIGHT 5 8  EL=5
LINE STRAIGHT 8 11 EL=14
```

```
LINE STRAIGHT 3 6  EL=9
LINE STRAIGHT 6 9  EL=5
LINE STRAIGHT 9 12 EL=14
*
* THE FOLLOWING CODE DEFINES MATERIAL PROPERTIES TO BE USED IN THE MODEL.
* THE FIRST MATERIAL SPECS CORRESPOND TO THE FIBER AND THE SECOND TO THE
* ALUMINUM MATRIX.  EACH SET CONTAINS THE CORRESPONDING COMMANDS FOR
* ELASTOPLASTIC ANALYSIS.  THE "TREF" COMMAND MUST BE SET TO 530.0 FOR THE
* QUENCH RUN AND 25.0 FOR THE SUBSEQUENT TENSILE DISPLACEMENT RUN.
MATERIAL 1 THERMO-ELASTIC TREF=530.0
    0.0   450E9  0.2  4.3E-6
 1000.0   450E9  0.2  4.3E-6
*MATERIAL 1 ELASTIC E=450E9 NU=0.2
*
MATERIAL 2 THERMO-PLASTIC TREF=530.0
    0.0   68.3E9  0.33  276E6  656E6  23.0E-6
 1000.0   68.3E9  0.33  276E6  656E6  23.0E-6
*MATERIAL 2 PLASTIC E=68.3E9 NU=0.33 Y=276E6 ET=656E6
*
* THE FOLLOWING CODE SELECTS GROUPS OF ELEMENTS IN THE MODEL AND ASSIGNS
* THEM PREVIOUSLY DEFINED MATERIAL PROPERTIES
EGROUP 1 TWODSOLID SUB=0 M=1
GSURF 5 6 9 8     EL1=6 EL2=5  NODES=4
GSURF 8 9 12 11   EL1=6 EL2=14 NODES=4
*
EGROUP 2 TWODSOLID SUB=0 M=2
GSURF 1 2 5 4     EL1=3 EL2=9  NODES=4
GSURF 2 3 6 5     EL1=6 EL2=9  NODES=4
GSURF 4 5 8 7     EL1=3 EL2=5  NODES=4
GSURF 7 8 11 10   EL1=3 EL2=14 NODES=4
*
* THE FOLLOWING CODE CONTAINS THE BOUNDARY CONDITION SPECIFICATIONS.  THE
* FOLLOWING CONDITIONS ARE APPLICABLE FOR THE ALIGNED FIBER MODEL.
* APPENDIX B CONTAINS A SECTION OF CODE ILLUSTRATING THE
* APPROPRIATE MODIFICATIONS FOR THE STAGGERED FIBER MODEL.
BO 111111 NODES
    12
BO 101111 NODES
    10 / 11
    34 TO 40
BO 110111 NODES
    3 / 6 / 9
    89 TO 112
*
CONSTRAINT
    1 3 3 3  TO  2 3 3 3
   13 3 3 3  TO 19 3 3 3
    1 2 10 2
    4 2 10 2
    7 2 10 2
   41 2 10 2 TO 64 2 10 2
*
* THE FOLLOWING COMMANDS DEFINE THE TYPE OF LOADING TO BE APPLIED TO THE
* MODEL.  THESE COMMANDS ARE USED IN CONJUNCTION WITH THE TIMEFUNCTION
* COMMANDS DISCUSSED PREVIOUSLY.  IT IS IMPORTANT TO NOTE THAT IF THE
* APPLIED LOADING IS STATIC (I.E. TIME INDEPENDENT) THEN THE TIME VALUES
```

```
* IN THE TIME FUNCTION COMMAND REPRESENT LOAD STEPS.
LOADS TEMPERATURE TREF=530
    1 1.0 1 TO 280 1.0 1
*
LOADS DISPLACEMENT
    3 3 1.0 2
*
* THE FOLLOWING COMMANDS ALLOW THE INPUT NODE AND ELEMENT CONFIGURATION
* FOR THE MODEL TO BE DISPLAYED ON THE SCREEN AS LONG AS THE "WORKSTATION"
* COMMAND IS COMMENTED OUT.
FRAME HEADING=UPPER XSF=1.0 YSF=0.5 XFMAX=22.5 YFMAX=17.0
MESH NODES=11 ELEMENT=1
*
ADINA
END
```

APPENDIX B. ADINA MODIFICATIONS FOR STAGGERED FIBER MODEL

The following modifications are used in the ADINA input file for the staggered fiber model analysis. Since many elements of the input file are unchanged from the aligned model, only required modifications are presented here.

```
TIMEFUNCTION 4
* DISPLACEMENTS FOR STAGGERED MODEL WITH RESIDUAL STRESSES
  0.0     0.0
  2.0     -.01075
  3.0     -.00851
  4.0     -.00401
  5.0     0.00500
  6.0     0.00952
  7.0     0.03226
*
TIMEFUNCTION 5
* DISPLACEMENTS FOR STAGGERED MODEL WITHOUT RESIDUAL STRESSES
  0.0     0.0
  1.0     0.00224
  2.0     0.00449
  3.0     0.00898
  4.0     0.01799
  5.0     0.02251
  6.0     0.04525
* BOUNDARY CONDITIONS
BO 101111 NODES
    7
BO 110111 NODES
    3 / 6 / 9 / 12
    91 TO 115
CONSTRAINT
* TOP CELL SURFACE REMAINS PLANAR AND IS SLAVED TO NODE 12
    1 3 12 3 -1.0  TO  3 3 12 3 -1.0
   13 3 12 3 -1.0  TO 19 3 12 3 -1.0
* BOTTOM CELL SURFACE REMAINS PLANAR
   10 3 12 3 1.0  TO 11 3 12 3 1.0
   34 3 12 3 1.0  TO 40 3 12 3 1.0
* AXIAL SIDEWALL CONSTRAINT
   41 3 65 3 -1.0
   42 3 64 3 -1.0
   43 3 63 3 -1.0
   44 3 62 3 -1.0
   45 3 61 3 -1.0
   46 3 60 3 -1.0
   47 3 59 3 -1.0
   48 3 58 3 -1.0
```

```
    4 3 57 3 -1.0
   49 3 56 3 -1.0
   50 3 55 3 -1.0
   51 3 54 3 -1.0
   52 3 53 3 -1.0
*
* LOAD COMMANDS
LOADS DISPLACEMENT
    12 3 -1.0 4
```

APPENDIX C. DATA REDUCTION PROGRAMS

The following programs were used to reduce the ADINA output file to data points to be plotted on stress-versus-strain curves.

```
C THIS PROGRAM READS THE ADINA OUTPUT FILE AND COMBINES THE STRESS VALUES
C WITH THE ELEMENTAL VOLUMES TO PRODUCE A VOLUME-AVERAGED VALUE OF AXIAL
C STRESS.
C
      PROGRAM TEST
      CALL INIT
      CALL READ
      STOP
      END
C
C THIS SUBROUTINE ZEROS OUT ARRAYS AND READS THE VOLUME DATA FILE.
C THE PARAMETER VARIABLES ARE: NUMBER OF ELEMENTS (NEL), NUMBER OF LOAD
C STEPS (LC) AND NUMBER OF ELEMENTS IN THE FIBER (NFBR).
C
      SUBROUTINE INIT
      PARAMETER (NEL=252,LC=6,NFBR=114)
      REAL SZ(1:NEL,1:4),SZBAR(1:LC),V(1:NEL),FBR(1:NFBR)
      COMMON // SZ,SZBAR,V,FBR
C
      DO 10 I=1,NEL
      V(I)=0.0
      DO 15 J=1,4
      SZ(I,J)=0.0
15    CONTINUE
10    CONTINUE
C
      DO 20 K=1,LC
      SZBAR(K)=0.0
      FBR(K)=0.0
20    CONTINUE
C
      OPEN (01,STATUS='OLD')
      DO 25 L=1,NEL
      READ (01,*,END=50) V(L)
25    CONTINUE
C
50    PRINT *, 'EOF VOL.DAT'
C
      RETURN
      END
C
C THIS SUBROUTINE READS THE FORMATTED ADINA OUTPUT FILE, AFTER THE HEADERS
C HAVE BEEN REMOVED, AND CALCULATES THE AVERAGE Z STRESS IN EACH ELEMENT
C BY AVERAGING THE FOUR STRESS VALUES AT THE GAUSS POINTS.  THIS AVERAGE
```

```
C STRESS IS MULTIPLIED BY ITS ELEMENTAL VOLUME AND SUMMED OVER THE ENTIRE
C VOLUME OF THE MODEL.  THE OUTPUT IS TWO FILES: ONE CONTAINING THE
C COMPOSITE STRESS VALUES AT THE GIVEN LOAD LEVELS AND ONE CONTAINING
C THE STRESS LEVELS IN THE FIBER AT THE SAME LOAD LEVELS.
C
      SUBROUTINE READ
      PARAMETER (NEL=252,LC=6,VOL=4.97,NFBR=114)
      REAL SZ(1:NEL,1:4),SZBAR(1:LC),V(1:NEL),FBR(1:NFBR)
      CHARACTER*8 STATE
      COMMON // SZ,SZBAR,V,FBR
C
      OPEN (02,STATUS='OLD')
      OPEN (03,FILE='V30.DAT',STATUS='NEW')
      OPEN (04,FILE='V30_FBR.DAT',STATUS='NEW')
C
      DO 20 K=1,LC
      SUM=0.0
      DO 25 L=1,NEL
      READ (02,*) IEL
      READ (02,21) INR,INS,STATE,SX,SY,SZ(L,1),SYZ,SVM,SMAX
      READ (02,*) SYS,SMIN
      READ (02,*)
      READ (02,21) INR,INS,STATE,SX,SY,SZ(L,2),SYZ,SVM,SMAX
      READ (02,*) SYS,SMIN
      READ (02,*)
      READ (02,21) INR,INS,STATE,SX,SY,SZ(L,3),SYZ,SVM,SMAX
      READ (02,*) SYS,SMIN
      READ (02,*)
      READ (02,21) INR,INS,STATE,SX,SY,SZ(L,4),SYZ,SVM,SMAX
      READ (02,*) SYS,SMIN
      READ (02,*,END=50)
      READ (02,*,END=50)
21    FORMAT (14X,I1,3X,I1,5X,A8,5X,4(E12.5,2X),5X,2(E12.5,4X))
C
      SBAR=((SZ(L,1)+SZ(L,2)+SZ(L,3)+SZ(L,4))/4.0)*V(L)
C
      SUM=SUM+SBAR
C
      IF (L.EQ.NFBR) THEN
      FBR(K)=SUM/VOL
      ENDIF
25    CONTINUE
      SZBAR(K)=SUM/VOL
20    CONTINUE
C
50    PRINT *, 'EOF DETECTED'
C
      DO 35 N=1,LC
      WRITE (03,*) SZBAR(N)
      WRITE (04,*) FBR(N)
35    CONTINUE
      RETURN
      END
```

```
C THIS PROGRAM CALCULATES ELEMENTAL VOLUMES BASED ON THE GEOMETRY OF THE
C FINITE-ELEMENT MODEL.  THE REQUIRED INPUTS ARE:
C             NX: NUMBER OF ELEMENTS IN THE MODEL IN THE HORIZ. DIRECTION.
C             NY: NUMBER OF ELEMENTS IN THE MODEL IN THE VERT. DIRECTION.
C             NFX: NUMBER OF FIBER ELEMENTS IN THE HORIZ. DIRECTION.
C             NFY: NUMBER OF FIBER ELEMENTS IN THE VERT. DIRECTION.
C             NFM: NUMBER OF ELEMENTS IN THE VERT. DIRECTION FROM THE
C                  MODEL MIDPOINT TO THE FIBER END.
C             NEL: NUMBER OF TOTAL ELEMENTS IN THE MODEL (NX x NY).
C             XF: RADIUS OF FIBER DIVIDED BY NFX.
C             XM: (RADIUS OF CELL - RADIUS OF FIBER) DIVIDED BY (NX-NFX).
C             YF1: (LENGTH OF FIBER - 0.5*LENGTH OF CELL) DIVIDED BY NFM.
C             YF2: 0.5*LENGTH OF CELL DIVIDED BY (NFY-NFM).
C             YM: (LENGTH OF CELL - LENGTH OF FIBER) DIVIDED BY (NY-NFY)
C
      PROGRAM CVOL
      PARAMETER (NX=9,NY=27,NFX=6,NFY=18,NFM=4,NEL=243,
     & XF=.1666,XM=.1633,YF1=.19,YF2=.16,YM=.1644)
      REAL VOL(1:NEL),V(1:NX,1:NY)
C
C INITIALIZE THE MATRICES
      DO 10 I=1,NX
      DO 10 J=1,NY
10    V(I,J)=0.0
C
      DO 15 I=1,NEL
15    VOL(I)=0.0
C
C CONSTRUCT THE V MATRIX AND MAP IT INTO THE VOL MATRIX.
C   *** TOP FIBER GROUP ***
      NID=1
      DO 20 L1=NFY,NFY-NFM+1,-1
      DO 21 K1=NFX,1,-1
      V(K1,L1)= ((XF*K1)**2 - (XF*(K1-1))**2)*YF1/2.
      VOL(NID)=V(K1,L1)
      NID=NID+1
21    CONTINUE
20    CONTINUE
C   *** BOTTOM FIBER GROUP ***
      DO 200 L10=NFY-NFM,1,-1
      DO 210 K10=NFX,1,-1
      V(K10,L10)= ((XF*K10)**2 - (XF*(K10-1))**2)*YF2/2.
      VOL(NID)=V(K10,L10)
      NID=NID+1
210   CONTINUE
200   CONTINUE
C   *** TOP RIGHT MATRIX ELEMENT GROUP ***
      DO 22 L2=NY,NFY+1,-1
      DO 23 K2=NX,NFX+1,-1
      V(K2,L2)=((XM*(K2-NFX)+XF*NFX)**2-
     &          (XM*(K2-1-NFX)+XF*NFX)**2)*YM/2.
      VOL(NID)=V(K2,L2)
      NID=NID+1
23    CONTINUE
22    CONTINUE
C   *** TOP LEFT MATRIX ELEMENT GROUP ***
```

```
      DO 24 L3=NY,NFY+1,-1
      DO 25 K3=NFX,1,-1
      V(K3,L3)= ((XF*K3)**2 - (XF(K3-1))**2)*YM/2.
      VOL(NID)=V(K3,L3)
      NID=NID+1
25    CONTINUE
24    CONTINUE
C   *** MIDDLE MATRIX ELEMENT GROUP ***
      DO 26 L4=NFY,NFY-NFM+1,-1
      DO 27 K4=NX,NFX+1,-1
      V(K4,L4)= ((XM*(K4-NFX)+XF*NFX)**2 -
     &           (XM*(K4-1-NFX)+XF*NFX)**2)*YF1/2.
      VOL(NID)=V(K4,L4)
      NID=NID+1
27    CONTINUE
26    CONTINUE
C   *** BOTTOM MATRIX ELEMENT GROUP ***
      DO 260 L40=NFY-NFM,1,-1
      DO 270 K40=NX,NFX+1,-1
      V(K40,L40)= ((XM*(K40-NFX)+XF*NFX)**2 -
     &             (XM*(K40-1-NFX)+XF*NFX)**2)YF2/2.
      VOL(NID)=V(K40,L40)
      NID=NID+1
270   CONTINUE
260   CONTINUE
C   *** CHECK TO ENSURE THE SUM OF THE ELEMENTAL VOLUMES MATCH THE ***
C   *** CALCULATED MODEL VOLUME AND WRITE THE OUTPUT TO A FILE.    ***
      VNUM= (((XF*NFX)+(XM*(NX-NFX)))**2)*((YF1*NFM)+
     &        (YF2*(NFY-NFM))+(YM*(NY-NFY)))/2.
C
      VCALC=0.0
      DO 30 N=1,NEL
      VCALC=VCALC+VOL(N)
30    CONTINUE
      PRINT *, 'VNUM=",VNUM
      PRINT *, 'VCALC=',VCALC
      DO 35 M=1,NEL
35    WRITE (10,*) VOL(M)
C
      STOP
      END
```

LIST OF REFERENCES

1. A.R.T. deSilva and G.A. Chadwick, *J. Mech. Phys. Solids*, **17**(1969) p.387.

2. G.J. Dvorak, M.S.M. Rao and J.Q. Tarn, *J. Comp. Mat.*, **7**(1973) p.194.

3. C.A. Hoffman, *J. Eng. Mat. Tech.*, **95**(1973) p.55.

4. G. Garmong, *Met. Trans.*, **5**(1974) p.2183.

5. J.K. Lee, Y.Y. Earmme, H.I. Aaronson and K.C. Russell, *Met. Trans.*, **11A**(1980) p.1837.

6. Y.Y. Earmme, W.C. Johnson and J.K. Lee, *Met. Trans.*, **12A**(1981) p.1521.

7. R.J. Arsenault and R.M. Fisher, *Scripta Metall.*, **17**(1983) p.67.

8. R.J. Arsenault, *Mat. Sci. Eng.*, **64**(1984) p.171.

9. R.J. Arsenault and M. Taya, *Proceedings, ICCM-V, AIME*, San Diego, edited by W.C. Harrigan, Jr., et al., (1985) p.21.

10. M. Taya and R.J. Arsenault, *Scripta Metall.*, **21**(1987) p.349.

11. V.C. Nardone and K.M. Prewo, *Scripta Metall.*, **20**(1986) p.43.

12. R.J. Arsenault and N. Shi, *Mat. Sci. Eng.*, **81**(1986) p.175.

13. P.J. Withers, W.M. Stobbs and O.B. Pedersen, *Acta Metall.*, **37**(1989) p.3061.

14. B. Derby and J.R. Walker, *Scripta Metall.*, **22**(1988) p.529.

15. I. Dutta, D.L. Bourell and D. Latimer, *J. Comp. Mat.*, **22**(1988) p.829.

16. I. Dutta, *Comp. Sci. Tech.*,(1990) (in press).

17. G.L. Povirk, A. Needleman and S.R. Nutt, *Mat. Sci. Eng.*, **A125**(1990) p.129.

18. T. Christman, A. Needleman and S. Suresh, *Acta Metall.*, **11**(1989) p.3029.

19. V. Tvergaard, *Acta Metall.*, **38**(1990) p.185.

20. V. Tvergaard, *Mat. Sci. Eng.*, **A125**(1990) p.203.

21. A. Levy and J.M. Papazian, *Met. Trans.*, **12A**(1990) p.411.

22. J.R. Brockenbrough and S. Suresh, *Scripta Metall.*, **24**(1990) p.325.

23. Y.Takao, T.W. Chou and M. Taya, *J. Appl. Mech.*, **49**(1982) p.536.

24. Y.Takao and M. Taya, *J. Comp. Mat.*, **21**(1987) p.140.

25. ADINA Product Manuals, Version 2.0 ADINA R&D Corp., Watertown, MA, December 1987.

26. K.J. Bathe, *Finite Element Procedures in Engineering Analysis,* pp. 301-400, Prentice-Hall, 1982.

27. M.R. Piggott, *Load Bearing Fiber Composites,* pp. 62-82, Pergamon Press, 1980.

28. R.J. Arsenault, *'Strengthening Mechanisms in Discontinuous SiC/Al Composites'*, in *Composite Structures,* edited by R.H. Marshall, 1987, p.70.

29. Y. Flom and R.J. Arsenault, *'Deformation in SiC/Al Composites'*, in *Mechanical Behavior of Materials,* edited by M.G. Yan, S.H. Zhang and Z.M. Zhang, 1987, p.1253.

INITIAL DISTRIBUTION LIST

		No. Copies
1.	Defense Technical Information Center Cameron Station Alexandria, VA 22304-6145	2
2.	Library, Code 52 Naval Postgraduate School Monterey, CA 93943-5002	2
3.	Professor Indranath Dutta Department of Mechanical Engineering Code ME/Du Naval Postgraduate School Monterey, CA 93943-5100	2
4.	Professor Gilles Cantin Department of Mechanical Engineering Code ME/Ci Naval Postgraduate School Monterey, CA 93943-5100	1
5.	Professor David Salinas Department of Mechanical Engineering Code ME/Sa Naval Postgraduate School Monterey, CA 93943-5100	1
6.	LT John Sims 2112 Louise Av. Monroe, NC 28110	2